MINERALOGY OF SULFIDE NODULES IN SOME IRON METEORITES

FREDERICK B. HENDERSON III

DEPARTMENT OF GEOLOGICAL SCIENCES
HARVARD UNIVERSITY
CAMBRIDGE, MASSACHUSETTS

JUNE, 1965

ABSTRACT

15446

Forty mineral phases occurring in sulfide nodules from the Canyon Diablo, Cosby's Creek, Hex River, Magura, Toluca, and Trenton iron meteorites are described. Of these phases, eighteen remain unidentified and are under current study. The characteristic occurrence of these phases in a nodule rim and core structure is described. Common compatible assemblages of these phases are noted, many of which appear to be high temperature assemblages.

Accessory phases, in general, have probably exsolved from the principal nodular mineral, troilite. A similar association and textural sequence of phases occurs in all the nodules studied and indicates similar conditions of formation. Several silicate-troilite intergrowths suggest a possible reaction between sulfide and silicate phases. The silicate phases may have been mechanically included in the nodules, or may have resulted from primary crystallization. Deformation textures were observed that indicate pre-terrestrial metamorphism. Alteration Fe-Ni-S phases, including pentlandite and "heazlewoodite", appear to represent Ni-metasomatism by diffusion of Ni into the nodule from adjoining primary nickeliferous phases during metamorphism.

Author

INTRODUCTION AND ACKNOWLEDGEMENTS

Sulfide nodules in iron meteorites have been described by many authors (e.g.: Cohen, 1884 and 1904; Perry, 1944). They have not been extensively studied, but apparently are common to most iron meteorites. They occur in

the host kamacite as irregular drop-like forms up to 13 cm. in diameter, which tend to be oval or elliptical in cross-section and grade into cylindrical forms. Several rarer irregular forms (e.g., horseshoe, T-shaped, etc.) may be observed in cross-section. The elliptical and cylindrical nodules tend to be oriented parallel to one another. Sulfide nodules contain many mineral phases which are otherwise uncommon to iron meteorites.

Ramdohr (1963) made the first application of standard metallographic techniques to the study of meteoritic opaque minerals in stony meteorites, and his descriptions include many minerals common to sulfide nodules in iron meteorites. He described eleven unidentified minerals. Most of these were not found in this study, probably because of genetic differences between stony and iron meteorites. The present paper describes the mineralogy of some sulfide nodules occurring in six iron meteorites, including the coarse octahedrites Canyon Diablo, Cosby's Creek, Magura, Toluca, and Trenton, and the ataxite Hex River, and it discusses some genetic problems concerning them.

The author's sincere appreciation is extended to Dr. Clifford Frondel, Harvard University, for the use of his meteorite specimens and the guidance, suggestions, and encouragement that he provided.
Dr. Cornelis Klein, Jr., Harvard University, contributed greatly by providing, in addition to many fruitful ideas, electron microprobe analyses for most of the mineral phases observed. Dr. James B. Thompson, Jr.,

James Fred Hays, and Elinor G. Henderson also contributed significantly by their suggestions stemming from their critical readings of the manuscript.

This study is a part of a program on meteorite research under NASA Grant No. NsG ~~283-63~~ 282.

MINERALOGY

DEFINITIONS AND IDENTIFICATION TECHNIQUES

The forty mineral phases observed are listed in Table I and include eighteen unidentified or tentatively identified phases, which are designated minerals A - R. The identified phases were determined by qualitative or semi-quantitative electron microprobe analysis and by their metallographic optical properties. Such techniques were insufficient for the positive identification of minerals A - R. Several of these phases may be new minerals or new variants of known minerals and are under continuing study.

Table II lists by meteorite the commonly observed compatible and incompatible mineral assemblages. Many of these assemblages appear to be high temperature assemblages ($>500^{o}C$).

Samples were ground and polished, and non-conductive samples were carbon-coated for electron probe analysis after optical examination. Metallographic microchemical tests were not applied because of the fine grain size and the complexity of many of the phase assemblages. The Talmadge hardness scale (Short, 1940) of A - G (very soft to very hard) is utilized in the descriptions.

Throughout this paper, the word analysis refers to the qualitative or semi-quantitative analytical methods used, and further study will include the refinement of the phase compositions through quantitative analytical methods. An ARL (Applied Research Laboratories) electron microprobe was used for qualitative determination of elements heavier

than sodium for most of the phases. Fe and S were compared to coexisting troilite (assumed stoichiometric FeS). Some Fe values were cross-checked with nearby kamacite (assumed 94.5 wt.% Fe). Ni was compared to kamacite (assumed 5.5 wt.% Ni). Other qualitatively determined elements (Cr, Mn, Zn, etc.), or undetermined elements (O, C, or N), were assumed to constitute the remainder of a phase containing semi-quantitatively determined Fe, Ni, or S. Because of these assumptions, and because no absorption, fluorescence, or atomic number corrections were applied, the analyzed values contain errors and are hence semi-quantitative at best.

GENERAL NODULE STRUCTURE AND TEXTURES

Primary Nodule Structures and Textures.

Figure 1 is a composite sketch illustrating the typical nodule structure. Most nodules are nearly spheroidal in form and consist of a core, composed mainly of troilite, and a rim. All nodules studied exhibit this rim and core structure, although some rims are only partially developed, as in Hex River. In all nodules, there is a characteristic sequential rim and core occurrence of the phases. The only exceptions to this sequential occurrence are graphite and cliftonite, which may occur throughout the core, rim, and extra-nodular kamacite (Fig. 6).

The typical nodule occurs in a large single crystal of kamacite, the principal phase of octahedrite meteorites. Proceeding inwards, the complete sequence is as follows (Fig. 1). Cohenite forms the outermost band intergrown with inner schreibersite (Fig. 3). The outermost cohenite and/or schreibersite may possess a subhedral outer form and extend along kamacite

cleavage planes. A cliftonite or graphite band is the next layer (Fig. 10), beneath which is a ferroan sphalerite and/or rim troilite band (Figs. 10, 11). Minerals H and I form the innermost rim phases at the rim-core interface (Fig. 19).

The cores are usually composed of troilite, which may occur alone as a single crystal or as several coarse crystals, or it may contain one of the following intergrowth assemblages: daubreelite exsolution laminae (Cosby's Creek, Fig. 14); graphic troilite-graphite (Toluca, Fig. 8); silicate-sulfide-magnetite-graphite-chlorapatite (Toluca, Fig. 26); or silicate fragments in an iron oxide matrix (Trenton, Fig. 29). All of the cores observed have a relatively smooth core-rim interface and are semi-spherical.

IDENTIFIED PHASES

1. Kamacite: Kamacite is isotropic and generally exhibits Widmanstätten structure and Neumann lines. Its color is iron (light bluish) grey, and it is relatively soft (C-). In comparison to troilite, analyses varied between 93 to 94.5 wt.% Fe and 5.5 to 7 wt.% Ni. The range of Ni content corresponds generally to the total meteorite range of 5.5 to 8.1 wt.% Ni given by Massalski (1962) for the Hex River, Magura, Canyon Diablo, and Toluca iron meteorites. Analyses indicate that the Ni content of kamacite, the principal meteorite phase in the specimens studied, is essentially uniform throughout a given specimen.

The kamacite occurs as large single crystals enclosing all nodules and containing taenite, plessite, and schreibersite exsolution laminae and blebs. Where normally intervening rim phases are absent, kamacite abuts against core troilite (Fig. 1). It occurs uniquely in the center of the troilite-schreibersite-daubreelite core in the Hex River specimen (Fig. 2). Kamacite is highly susceptible to terrestial oxidation, and iron oxides commonly replace it along fractures and cleavages.

2. Taenite: Taenite is slightly harder (D+) than the enclosing kamacite, and it is isotropic and yellowish white grey. Taenite is richer in Ni than coexisting kamacite. Taenite forms the principal exsolution lamdnae on kamacite cleavage planes in all specimens studied. It is concentrated around some outer nodule rims. Taenite occurs with plessite and schreibersite and is more resistant to oxidation than the enclosing kamacite.

Plessite, the eutectoid intergrowth of kamacite and taenite, was observed in the Canyon Diablo, Trenton, and Toluca specimens. In oxidized portions, taenite forms intergrowths with magnetite and limonite which replace the kamacite portion of the plessite.

3. Schreibersite: Harder (G) than kamacite and taenite, schreibersite is tin white with a rose cream tint which distinguishes it from tin white cohenite. Schreibersite is weakly anisotropic and pleochroic. Its greater hardness and brittleness is exhibited by more extensive fracturing and jointing than is found in adjacent phases (Fig. 3). Analyses indicate that schreibersite contains 15-25 wt.% Ni and corresponds to the composition $(Fe,Ni)_3P$.

Schreibersite is the principal rim phase. It rims all other nodule and rim phases, except cohenite, which is intergrown with it or forms a band between rim schreibersite and extra-nodular phases. The schreibersite band is usually a single crystal and may project out along kamacite cleavage planes. It occurs less commonly as a rim fragment mechanically included in the core (Figs. 4, 5). It also occurs as exsolved laminae and discrete euhedral grains (rhabdites) in extra-nodular kamacite. Schreibersite is resistant to oxidation and generally occurs with secondary magnetite and limonite in oxidized zones.

4. Cohenite: This phase is whiter than, but easily confused with, schreibersite. It is tin white and weakly anisotropic and pleochroic. Cohenite is easily mistaken for mineral F, although it is softer (E) and has less distinctive anisotropism. Cohenite characteristically exhibits less fracturing and jointing than adjacent schreibersite (Fig. 3). The composition of cohenite is generally uniform, and compared to troilite, its iron content approximates that of stoichiometric Fe_3C. Analyses indicated trace amounts of nickel (less than 1 wt.%) and the absence of any other element, notably S and P. It should be noted that nodular cohenite appears to be essentially nickel-free.

Cohenite commonly occurs as the outermost rim phase, situated between kamacite and schreibersite or troilite (Fig. 3), or intergrown with rim schreibersite. It was observed as a rim phase in all specimens.

5. Graphite (and Cliftonite): Graphite is very common in both rim and core assemblages, occurring as dark to brownish grey, very soft (A), and strongly anisotropic and pleochroic micaceous hexagonal plates. It occurs as crystalline or amorphous aggregates within the rim schreibersite, cohenite, and troilite (Fig. 6). Graphite forms platy aggregates, sometimes deformed (Fig. 7), in the Toluca silicate-sulfide core intergrowths. Its principal core occurrence is as graphic intergrowths with troilite, with the graphite plates oriented along cleavage planes in the coarse grained troilite host (Fig. 8). Other minor exsolved phases such as daubreelite, ferroan alabandite, and pentlandite are found in these graphic intergrowths. The relative proportions of troilite and graphite vary, forming bands of different total composition (Fig. 9) with up to 50 volume % graphite. Graphite occurrences were observed in all the specimens studied, except the ataxite, Hex River.

Cliftonite is a name applied to a texturally and genetically distinct form of graphite, and is the subject of a detailed study by Frondel (1965). "Cliftonite" graphite occurs oriented in cubical and cubo-octahedral aggregates (Figs. 6,10,11,38), which are euhedral against all other phases, relatively large (up to 0.1 mm.), and ubiquitous throughout the mineralogy of the Toluca specimens. Cliftonite occurs as discrete aggregates in extra-nodular kamacite (Fig. 6), in or with all the rim phases, and in the troilite of the graphic troilite-graphite intergrowths. It is principally associated with rim graphite, schreibersite, cohenite, and troilite. In one Toluca specimen, it forms a thick crystalline band adjacent to schreibersite and troilite (Fig. 10). It was observed in the Cosby's Creek graphite rim. Cliftonite is probably pseudomorphic after an early

crystallizing phase, perhaps primary diamond (Frondel, 1965). However, if diamond were the primary phase, it would be incompatible in its Toluca occurrence with anorthite, since the anorthite decomposes at 30 kilobars pressure, which is below the stability field for diamond at temperatures greater than 400°C (Boyd and England, 1961).

6. Troilite: Troilite is brownish brass yellow, but varies to yellower or browner shades. It is moderately soft (D) and apparently sensitive to stress. Many examples of physical deformation of troilite were observed. These deformation zones, described in a later section, commonly show partial or extensive alteration of troilite by Fe-Ni-S phases, notably pentlandite (Fig. 12). In some specimens, angular troilite breccias occur in a magnetite matrix (Fig. 5).

Troilite is probably stoichiometric FeS (1:1 pyrrhotite) having crystallized in the presence of an iron phase (kamacite). It exhibits none of the crystallographic variations (see Gehlen, 1963) common to terrestial pyrrhotites, as noted by Ramdohr (1963). Two orientations of pentlandite and daubreelite laminae in troilite cleavage planes were observed in this study. Three-fold orientation (Fig. 13) was noted in most specimens (especially Canyon Diablo and Toluca), however, perpendicular laminae occur in the Cosby's Creek specimen (Fig. 14).

The composition of troilite is generally considered to be stoichiometric FeS (Ramdohr, 1963; Mason, 1962; Perry, 1944, and Gehlen, 1963). Qualitative analytical calculations for wt.% Fe in magnetite, limonite, pyrite, and the Fe-Ni-S minerals, using adjacent assumed stoichiometric troilite as a standard, were reasonably close to the correct values. However, significant

variations in color suggest that the troilite composition may vary. Such variations might include the presence of Ni or Ti (Keil and Fredrikson, 1963). However, only Fe and S were detected in analyses made of "off-color" and normal troilites.

Troilite is the principal phase of all the observed nodule cores forming 90-95 volume % of most cores. In specimens containing intergrowths of silicate-sulfide (Toluca), silicate-iron oxide (Trenton), or graphic troilite-graphite (Toluca), it forms 50-90 volume % of the cores. Core troilite usually occurs as either a single crystal or several coarse grained crystals.

Graphic troilite-graphite intergrowths have been described above. In the troilite-silicate-graphite-magnetite-chlorapatite intergrowths in Toluca, the troilite occurs in five forms: 1) discrete grains intergrown with similar sized silicate grains (Fig. 6); 2) blebs occurring within the silicate grains and often containing smaller blebs of ferroan alabandite, daubreelite, pentlandite, and mineral L; 3) myrmekitic intergrowths with hypersthene and occasionally mineral B (Figs. 15,16); 4) veinlets, sometimes containing pentlandite, which cut through earlier silicate grains and troilite blebs (Fig. 17); and 5) spherical "drops", which contain small blebs of pentlandite, ferroan alabandite, and daubreelite and occur in a vein matrix of chlorapatite and primary magnetite (Fig. 18).

Blebs and exsolution laminae of pentlandite, ferroan alabandite, daubreelite, native copper, and minerals A, B, D, E, and L commonly occur within larger troilite grains in all specimens studied. Rim troilite occurs in Toluca specimens (Fig. 19) in the inner rim and partially separated from the core by minerals H and I. Where rim troilite occurs, the core is composed of either silicate-sulfide or graphic troilite-sulfide intergrowths.

7. Pyrite: Pyrite occurs uniquely in one Trenton specimen as several large (0.25 mm.) masses oriented with respect to a cleavage direction in a host troilite grain (Fig. 20). The pyrite is isotropic, hard (F), and brass yellow. Compared to coexisting troilite, analysis indicates an Fe content consistent with stochiometric FeS_2, and no elements besides Fe and S were detected. Mineral J everywhere rims the pyrite at the pyrite-troilite interface.

8. Pentlandite: The occurrence of pentlandite and related Fe-Ni-S phases is the subject of a paper in preparation. Pentlandite is relatively soft (D) and isotropic. It is bronze yellow, with some variation to lighter and darker shades. Stoichiometric pentlandite is $(Fe,Ni)_9S_8$, and semi-quantitative analyses indicated a generally constant metal/S ratio of 9/8 compared to troilite and kamacite. The Fe/Ni ratios tend to be near 5/4, but have a range of 1/1 to 2/1. Pentlandite is probably close to stoichiometric, but some compositional variation may be the cause of its color variation. No elements other than Fe, Ni, and S were detected.

Pentlandite occurs in all specimens except Hex River and Canyon Diablo. Pentlandite, associated with daubreelite and ferroan alabandite, occurs as primary blebs throughout the troilite cores. They are usually concentrated near the core periphery (Fig. 21) or near graphite in graphic troilite-graphite intergrowths (Fig. 8). One Toluca specimen exhibited exsolved pentlandite laminae along troilite cleavage planes parallel to exsolved daubreelite laminae. Pentlandite grains commonly occur in troilite blebs and veinlets within silicate grains in the Toluca silicate-sulfide assemblages (Fig. 18).

The principal occurrence of pentlandite, sometimes with other Fe-Ni-S phases, is as a troilite alteration phase probably caused by Ni-metasomatism along zones of weakness, such as shear zones (Figs. 11,22), fractures (Fig. 14), and cleavage planes (Fig. 13). The Fe-Ni-S phases are most abundant on core peripheries or in rim troilite, and they tend to be less abundant or missing toward the core center (Fig. 23). They are best developed adjacent to Ni-bearing phases, especially schreibersite and kamacite, and are only weakly developed or absent adjacent to Ni-free cohenite (Fig. 24) or to an intervening inner graphite rim (Fig. 6). Metasomatic pentlandite is common in all specimens except Hex River and Canyon Diablo. Such pentlandite occurrences are attributed by Ramdohr (1963), Kullerud (1963), and Mason (1962) to the release of Ni from Ni-bearing phases by terrestrial oxidation and aqueous reaction with troilite to form pentlandite. The author favors the formation of these pentlandites by pre-terrestrial nickel-metasomatism.

9. Daubreelite: Daubreelite is isotropic and harder (E) and less fractured than troilite. It is brownish yellow (darker than troilite) with a greenish tint. In comparison with troilite, analyses generally indicated Fe and S values consistent with stoichiometric $FeCr_2S_4$. As Cr was the only other element generally detected, daubreelite is probably stoichiometric.

All specimens contained daubreelite. It occurs in aggregates with ferroan alabandite and pentlandite in troilite near core peripheries (Fig. 21). Daubreelite commonly forms exsolution laminae oriented along troilite cleavage planes, especially in the Cosby's Creek specimen (Fig. 14).

In this specimen pentlandite is closely associated with the daubreelite laminae, but is considered a later alteration phase of the enclosing troilite.

Some Toluca specimens contain daubreelite and chromite, but they are never directly associated. Chromite occurs as large discrete grains or exsolved blebs in the silicate assemblages, whereas the daubreelite occurs separately as exsolved grains within troilite blebs in silicate grains and in rim troilite. Daubreelite probably has exsolved from troilite, and chromite perhaps formed with the silicates in the presence of oxygen.

10. Manganiferous daubreelite: This phase is whitish yellow brown and lighter than normal daubreelite. In the Cosby's Creek specimen it is white tan and occurs as exsolution laminae along cleavage planes parallel to, but separate from, normal daubreelite-containing cleavage planes in troilite. It is otherwise similar in appearance to normal daubreelite. Analyses of manganiferous daubreelite indicate a variable but significant Mn content. Keil and Fredrikson (1963) report a similar low (1.0 wt.%) Mn-bearing daubreelite in the Norton County achondrite.

Manganiferous daubreelite was observed in the Canyon Diablo and Hex River specimens. In the Hex River specimen it uniquely occurs as small (5-15μ) grains intergrown with similar sized grains of mineral F in an aggregate of coarser grained troilite. This assemblage forms the core (Fig. 2). The manganiferous daubreelite is irregularly distributed throughout, but forms 25 volume % of the core. Ferroan alabandite and normal daubreelite occasionally replace the manganiferous daubreelite.

11. Ferroan sphalerite: Ferroan sphalerite is isotropic, relatively soft (D), and it is darker grey than stoichiometric sphalerite (ZnS). It exhibits a dark brown internal reflection and shows little or no fracturing or jointing. Analyses indicate that ferroan sphalerite may contain more than 50 mole % FeS, which would be indicative of high temperature, 580-800°C, (Barton, Toulmin, 1963). Only Fe, Zn, and S were detected by analysis.

Ferroan sphalerite is a common rim phase in some Toluca specimens, occurring as a single crystal band between outer rim schreibersite, cohenite, and cliftonite and inner rim troilite (Figs. 10, 11). Mineral O occurs as fine grained exsolution blebs in ferroan sphalerite. Ferroan sphalerite occasionally occurs as small grains with ferroan alabandite and daubreelite in the core, especially in the silicate-sulfide intergrowths.

12. Ferroan alabandite: This phase is light medium grey, slightly lighter than ferroan sphalerite. It is isotropic and softer (C) than troilite. Keil and Fredrikson (1963) and Ramdohr (1964) describe a similar Mg-, Fe- bearing meteoritic alabandite phase. Analyses of ferroan alabandite suggest a composition of (Mn,Fe)S with a Mn/Fe ratio of about 6/1. Ferroan alabandite is common to all specimens except Cosby's Creek. It generally occurs with fine grained pentlandite and daubreelite as blebs along the core troilite peripheries (Fig. 21), or along graphite intergrowths with troilite (Fig. 8). Mineral N occurs as exsolution blebs in many ferroan alabandite grains.

13. Native copper: Native copper is soft (B), isotropic, and copper colored. It occurs in troilite as small (0.20 x 0.02 mm.) grains. It is a minor phase in the Cosby's Creek, Trenton, and Toluca specimens, occurring in blebs along the troilite core peripheries, where it is generally associated with a grey copper oxide (?) phase in adjacent late iron oxide veins (Fig. 13). In the Toluca specimen native copper occurs with the Cu-Fe-S minerals A, D, and E on the periphery of rim troilite (Fig. 25).

14. Hypersthene: Hypersthene is in reflected light lighter grey than anorthite, the other commonly occurring silicate phase. Though generally rounded in form, some elongated grains exhibit prismatic cleavage. It is hard (G), medium grey, and possesses a strong yellow brown internal reflection in oblique light.

An X-ray diffraction pattern (Table III) of a mixture of the Toluca silicate-sulfide intergrowth phases includes most of the principle hypersthene lines. Optical verification of the presence of hypersthene is indicated by the following observations made on crushed grains: low birefringence; prismatic form with parallel extinction; yellow brown color; and $1.70 < N_x$ and $N_z < 1.72$. The observed indices indicate a compositional range of 56-60 mole % $MgSiO_3$: (Winchell, 1961, p. 406).

Hypersthene is one of the two principal silicate phases in the Toluca silicate-sulfide assemblages, which compose up to 85 volume % of the cores. Hypersthene and anorthite, in roughly equal proportions, form about 65 volume % of the intergrowths (Figs. 26, 27). They occur as equigranular, anhedral to subhedral grains, 0.1 to 0.5 mm. in size. Both silicates are

intergrown with micaceous graphite. Semi-spherical and elongated troilite blebs occur in both silicates (Figs. 17,26,27), or are oriented along the silicate interfaces, which also contain primary magnetite (Fig. 28). In some sections, the troilite forms parallel oriented "trains" of blebs cutting indiscriminantly across all other phases (Fig. 26) and may represent healed fractures. Many hypersthene grains contain troilite blebs as an intimate myrmekitic intergrowth (Figs. 15, 16). Hypersthene also occurs as fragments with mineral R and anorthite in an iron oxide matrix in some Trenton cores.

15. Olivine: Olivine is very similar in polished section to hypersthene, but it has a greenish internal reflection. Analysis indicates the presence of Mg, Fe, and Si. The intergrowth mixture X-ray diffraction pattern (Table III) contains all of the principal olivine lines (A.S.T.M. # 7-0159; 64 mole % Mg_2SiO_4). Optical verification of the identification of this phase was based on the following observed properties of crushed grains: parallel extinction; light green color; relatively high birefringence; $1.70 < N_x$ and $N_z < 1.74$. These indices indicate a composition of about 65 mole % Mg_2SiO_4 (Deer, Howie, and Zussman, 1962).

Olivine was observed in the center of the Toluca silicate-sulfide core. Its grain size is larger than the other silicate grains. It encloses some troilite blebs, but no myrmekitic troilite-olivine intergrowths were observed. This phase composes an estimated 5 volume % of the core intergrowth.

16. Anorthite: Anorthite is hard (G), dark grey (darker than hypersthene), anhedral, and exhibits no internal reflection. Analyses indicated the presence of Ca, Al, and Si. The intergrowth mixture X-ray diffraction pattern (Table III) includes all the principal anorthite lines. The following optical properties observed in crushed grains verified the identification of this phase as a calcic plagioclase, probably anorthite: low birefringence; colorless; and in general, $1.580 \leq N_x$ and $N_z < 1.590$, which corresponds to a composition range of an_{90}-an_{100} (Winchell, 1961, p. 280).

Anorthite is the other principal silicate in the Toluca silicate-sulfide assemblages. Its general occurrence is described above with hypersthene. Troilite blebs are enclosed in anorthite, but no myrmekitic anorthite-troilite intergrowths were observed. Chlorapatite-magnetite intergrowths occur with both silicates, but tend to be associated with anorthite. Anorthite is found as fragments and in fragmented intergrowths with hypersthene and mineral R in the Trenton silicate-iron oxide assemblages.

17. Ureyite: This new meteoritic pyroxene was observed as a euhedral grain in kamacite adjacent to the Hex River nodule rim. It is dark grey and pleochroic in reflected light, hard (G), small (25μ), transparent, and exhibits a brilliant green internal reflection. Analysis indicated the presence of Cr, Si, and minor Ca. The analysis did not investigate the presence or absence of Na, but this phase is concluded to be ureyite ($NaCrSi_2O_6$), described by Frondel and Klein (1965), with minor Ca present in solid solution.

18. Chromite: Chromite is hard (G), subhedral, isotropic, light grey (lighter than hypersthene), and exhibits no internal reflection. Analyses indicated the presence of Fe and Cr only. Chromite is considered incompatible with the Cr-bearing sulfides daubreelite, manganiferous daubreelite, and mineral P, because it was never observed associated with these phases although they occur in the same nodules.

Chromite is a minor phase that is common in the Toluca silicate-sulfide assemblages. Individual subhedral grains occur randomly throughout the assemblage, but tend to concentrate near the assemblage periphery. The chromite grain size is slightly larger than that of the average silicate phase. Chromite also occurs as blebs in silicate phases and as myrmekitic intergrowths with hypersthene (Fig. 15).

19. Chlorapatite: This phase is medium grey (slightly lighter than magnetite), softer ($\sim$E) than the silicate phases, and it exhibits a bright yellow brown internal reflection. Analyses indicated the presence of Ca, P, and Cl. In addition, the intergrowth mixture X-ray diffraction pattern (Table III) includes all the principal chlorapatite lines.

Chlorapatite is common to the Toluca silicate-sulfide assemblages, in which it is always intimately veined by primary magnetite (Fig. 18). It is generally associated with anorthite. Chlorapatite forms a crosscutting vein in the wholly silicate-sulfide core. This vein contains spherules of troilite, which may have formed as immiscible liquid drops (Fig. 18). The vein is continuous, but the chlorapatite is abruptly substituted for by graphite (Fig. 27).

20. Ilmenite: Ilmenite is pleochroic (light grey to purplish brown grey) and strongly anisotropic (light grey to brown). It is hard (G) and exhibits no internal reflection. Analysis indicated the presence of Fe and Ti only. Ilmenite intergrown with primary magnetite was observed as fragments along with silicate fragments in some Trenton cores (Fig. 29). The ilmenite and primary magnetite show no evidence of replacement by the matrix iron oxides.

21. Magnetite: Magnetite is ubiquitous in all sections studied. Most magnetite is secondary and occurs in veins and fractures which cut all primary phases or along their interfaces. Secondary magnetite and associated limonite are believed to be terrestial in origin through oxidation either by passage through the atmosphere (most secondary magnetites) or by weathering following impact (most limonites).

However, some magnetite is clearly primary, intergrown with silicate and phosphate phases. Primary and secondary magnetite are similar in their optical properties. Both are medium grey (lighter than limonite), hard (F), isotropic, and exhibit no pleochroism or internal reflection. Analyses indicate up to about 6 wt.% Ni substituting for Fe, which would correspond to 25 mole % trevorite ($NiFe_2O_4$). Primary magnetite is light medium grey and contains little or no Ni. Secondary magnetite contains 0 to 6 wt.% Ni, and as the Ni content increases, the color becomes a brownish grey.

Primary magnetite forms intimate intergrowths with pyroxene or chlorapatite (Fig. 28 and Fig. 18), or it occurs as fine veins on silicate grain boundaries (Fig. 28). Most of the magnetite in the silicate-troilite-graphite-chlorapatite-magnetite intergrowths in the Toluca specimens is considered primary.

Secondary magnetite is commonly superimposed on primary magnetite making their optical distinction difficult. But secondary magnetite is usually associated with limonite, and both secondary phases cut the primary phases.

Brecciated troilite occasionally occurs in a matrix of magnetite without limonite, and the troilite grains are sharply angular with no evidence of replacement (Figs. 4, 5). This troilite-magnetite breccia may be primary or may represent oxidation during atmospheric entry.

Secondary magnetite is easily recognized when associated with limonite in fractures crosscutting primary phases (Figs. 19, 22, 42, 43, 44). In general, oxidation is a selective process with the preferred replacement of kamacite > taenite > pentlandite > schreibersite > cohenite. The more resistant phases are commonly associated with secondary magnetite and limonite along zones of weakness such as major structural boundaries (i.e., rim band, rim-core, and rim-kamacite interfaces; Figs. 10, 19), fracture systems (Fig. 4), cleavage planes (Figs. 13, 14), shear zones (Fig. 22), deformation and recrystallized zones (Fig. 12), and pentlandite alteration zones (Figs. 13, 14, 22). Hence, secondary magnetite occurs with most phases in this study.

Some occurrences are quite complex. In one Toluca specimen, perhaps near the atmospheric fusion crust, an oxidized troilite nodule contains secondary magnetite of varying Ni content and color, mineral E (ferroan trevorite ?), limonite, and remnant troilite and pentlandite (Fig. 30).

Portions of two Trenton cores contain silicate fragments in a magnetite matrix with minor limonite (Fig. 29). It is not known whether this magnetite is primary or secondary.

22. Limonite: Limonite varies considerably in form and composition. It is generally dark grey and very fine grained. It commonly appears soft due to fine crystallinity, brittleness, and open spaces. It is distinguished from associated secondary magnetite by its darker color, pleochroism (medium to dark grey), anisotropism, and dull brown internal reflection. In addition, limonite tends to cut or replace both primary and secondary magnetite. Analyses of homogeneous limonite indicated the presence of some Ni, up to 5 wt.%, in addition to Fe.

UNIDENTIFIED OF TENTATIVELY IDENTIFIED PHASES

23. Mineral A: This phase is brass yellow (lighter than pentlandite) and weakly anisotropic. It appears softer ($\sim$ C+) than troilite. The grain size of mineral A is less than 6μ, which prevented unambiguous analysis.

Mineral A occurs in a Toluca specimen in troilite, partially rimming native copper and minerals D and E, and as discrete grains along the troilite rim near other Cu-bearing phases (Fig. 25). It may also occur as fine grains

in several troilite blebs in Toluca silicate phases. Because of its optical properties and its association with other Cu-Fe-S phases, mineral A may be chalcopyrite or a member of the non-stoichiometric, high temperature chalcopyrite phase region (Yund, Kullerud, 1960). In rimming mineral E (bornite ?) in troilite, mineral A may be a reaction rim phase.

24. Mineral B: Mineral B is hard (G), white grey, isotropic, with no internal reflection. It is generally euhedral, occurring in equant form showing two cleavages. Analysis detected only Ti and mineral B may be rutile, as suggested by the Toluca silicate-sulfide intergrowth X-ray diffraction pattern (Table III), which contains all the principal rutile lines.

Mineral B is a minor phase in the Toluca silicate-sulfide assemblages as blebs in the silicates (Fig. 28) and myrmekitic intergrowths with hypersthene (Fig. 15). In some specimens it forms euhedral grains in troilite. The Cosby's Creek specimen contains two grains of mineral B with graphite and schreibersite in the core troilite periphery.

25. Mineral C: This phase is hard (G), isotropic, and very dark brownish black with no internal reflection. Because of its similarity to and association with Ni-bearing magnetite and its much darker color, mineral C may be a Ni-rich member of the series magnetite ($FeFe_2O_4$) - trevorite ($NiFe_2O_4$). Mineral C is intergrown with secondary magnetite of varying Ni content and lighter grey color in the oxidized Toluca nodule described above (Fig. 30).

26. Mineral D: Mineral D is a light olive grey, subhedral, softer (C) than troilite, and anisotropic, with polarization colors of dark blue grey to light yellow grey. Its grain size is about 5μ, obviating conclusive analysis. It is the color of chalcopyrrhotite (Ramdohr, 1963), but it is anisotropic. Mineral D might be chalcopyrrhotite or vallerite (Ramdohr, 1963), or it may be cubanite, with which it is most optically similar. It occurs in the Toluca rim occurrence of copper-bearing phases in troilite adjacent to native copper and partially rimmed by mineral A (Fig. 25).

27. Mineral E: This phase occurs in troilite in the Toluca Cu-rich rim assemblage (Fig. 25), and is apparently isotropic and varies from pink blue to anomalous dark blue. It is softer ($\sim$B) than troilite and it is rimmed by mineral A (chalcopyrite ?). The largest grain observed was multicolored in blues and about 12μ in size. Analysis indicated the presence of Cu, Fe, and S. This phase resembles bornite or the high temperature bornite solid solution phase region studied by Yund and Kullerud (1960), Kullerud (1960), and Brett (1963).

28. Mineral F: This phase is common to most specimens in rim association with normal schreibersite and cohenite. Analyses indicated the presence of Fe, Ni, and P, with a metal/P ratio of 3/1; hence, it is probably a member of the schreibersite solid solution series Fe_3P-Ni_3P (Clark, 1961). It is whiter than normal schreibersite and lacks the rose cream tint, but is otherwise optically similar.

Mineral F was distinguished primarily by analysis, which indicated considerably more Ni than in normal schreibersite. It occurs in the Canyon Diablo, Hex River (Fig. 2), Magura, Toluca, and Trenton specimens.

29. Mineral G: Mineral G was observed in the Magura specimens and possibly in one Toluca specimen. The Magura specimens are highly brecciated and the troilite is extensively replaced by Fe-Ni-S phases, notably pentlandite and mineral L. Mineral G occurs as an apparent gradational phase between schreibersite and pentlanditized troilite (Fig. 31). It is anisotropic and varies from pale yellow white to yellow. Its boundaries are poorly defined. Analyses were highly variable, which may be due to its fine grained occurrence and to interference from neighboring phases. The analyses indicated the presence of Fe, Ni, P, and possibly S. Mineral G may be a reaction rim phase between schreibersite and troilite or pentlandite, but it could also be an unrecognizable mixture of these phases. It is generally less fractured or jointed than adjacent schreibersite. Mineral G contains zig-zag partings similar to Ramdohr's new mineral A (1963).

30. Mineral H: Mineral H is closely related to mineral I. Mineral H is coarsely grained (up to 0.28 mm.), anhedral, transparent, isotropic, and very dark grey. In refracted and transmitted light, it exhibits a brilliant apple green internal reflection and color. It appears to be harder than associated sulfides, but it is brittle and shows extensive fracturing. Analyses detected only Ni. The Ni content, compared to kamacite (assumed 5.5 wt.% Ni), is about 65 wt.% Ni. This phase may be bunsenite (NiO).

Mineral H was observed only in the Toluca specimens as the innermost rim phase between the graphic troilite-graphite core and all other rim phases (Fig. 19). It occasionally extends into or is wholly contained in the graphic troilite-graphite intergrowth. In two occurrences, there is a fine grained, similar appearing, coexisting, platy phase, which may or may not be a separate phase.

31. Mineral I: Minerals H and I appear identical in reflected light, but in refracted or transmitted light, mineral I exhibits a strong red brown internal reflection. Analyses indicated less Ni than mineral H and a significant Fe content. Both phases occur in the same rim-core interface in the same Toluca specimen, but the bands of these two phases are monomineralic and are never observed as being contiguous. Mineral I may be a compositional variety of mineral H, but they are easily distinguished and are separated in this paper.

32. Mineral J: Mineral J occurs as oriented laminae within pyrite and along the pyrite-troilite interface in one Trenton specimen described above (Fig. 20). It is black, isotropic, and appears softer than pyrite. Its maximum width is 7 microns. Analysis indicated the presence of Fe only, and no S. The iron content was the same as for pyrite, which is too low for either magnetite or limonite.

33. Mineral K: Mineral K is isotropic, slightly harder than pentlandite (~E), and white or pale yellow bronze. Analyses indicated the presence of Fe, Ni, Co, and S, and it may be a cobaltian pentlandite. Mineral K occurs sparsely near core peripheries associated with other minor

phases such as ferroan alabandite and native copper in the Toluca and Cosby's Creek specimens. In the Cosby's Creek specimen mineral G also appears as a late veining alteration filling and cutting earlier pentlandite veins (Fig. 32).

34. Mineral L: Mineral L is a common alteration of troilite in the Toluca specimens, associated with alteration pentlandite and mineral M. Mineral L also occurs in the Cosby's Creek, Magura, and Trenton specimens. It is yellow brown to brown grey, isotropic, and darker and harder ($\sim$E) than pentlandite and troilite. Analyses indicate the presence of Fe, Ni, and S. Ten semi-quantitative analyses indicated a compositional range of $(Ni,Fe)_3S_2$ (heazlewoodite) - $(Ni,Fe)_7S_4$ (metal-rich heazlewoodite). This general range corresponds to the high temperature phase region $(Ni,Fe)_{3\pm x}S_2$ (Kullerud, 1963), with a range of x values of +0.16 to +0.62. The Fe/Ni here observed were generally 1/6, but varied to 1/2. Natural heazlewoodite (stoichiometric Ni_3S_2) exists below 550°C and was not observed in this study. Until the compositional range of this phase (or phases) is established quantitatively, it is tentatively designated as high temperature "heazlewoodite". The dark brown Ni-rich "heazlewoodite" is similar to Ramdohr's new mineral E (1963).

Mineral L occurs in veins and fractures, which are 5-15 μ wide and contain troilite and pentlandite. Pentlandite is closely associated with "heazlewoodite"; both commonly replace troilite adjacent to Ni-rich rim phases (Figs. 33-36). In extensively Ni-metasomatized troilite, pentlandite, and "heazlewoodite" crosscut each other in a complex manner, sometimes occurring on different fracture sets implying a time separation (Figs. 35, 36).

"Heazlewoodite" is generally replaced by pentlandite (Figs. 33, 34). Kullerud (1963) reports that there is no evidence in nature of his experimental "heazlewoodite" phase region, or of his conclusion that "heazlewoodite" and troilite react to form pentlandite at 610°C, 1 atm., which is stable at lower temperatures (also see Bell, England, and Kullerud, 1964). The apparent replacement of "heazlewoodite" and troilite by pentlandite in these specimens may be a natural occurrence of these reactions.

35. Mineral M: Mineral M occurs with mineral L and pentlandite replacing troilite along complex fracture systems adjacent to schreibersite in some Toluca specimens (Fig. 37). It is harder (E) than pentlandite and is copper brown. It is strongly anisotropic with polarization colors of copper- and blue-grey. Analysis indicates a metal/S ratio of higher than 3/1, and a Fe/Ni ratio of 1/6. Such a composition corresponds to no known phase and plots on the Fe-Ni-S diagram in the two phase field $FeNi_3$(awurite) - Ni_3S_2(heazlewoodite) (Kullerud, 1963). Mineral M appears to replace mineral L ("heazlewoodite") and perhaps pentlandite, and it may be an unknown phase representing a high temperature reaction between these phases.

36. Mineral N: Minerals N and O were observed in most specimens, especially Toluca, and are fine grained ($<5\mu$) unidentified grey phases. They are lighter grey than either ferroan alabandite or ferroan sphalerite, and they were distinguished by their distinctive associations. Mineral N forms fine exsolution blebs in ferroan alabandite (Fig. 38). It is light grey, isotropic, and apparently soft ($\sim$B).

37. Mineral O: Mineral O is a light grey phase similar to mineral N. It is lighter grey and probably softer than ferroan sphalerite in which it occurs as small exsolution blebs. It was observed only in the Toluca specimens.

38. Mineral P: This phase differs from similar appearing pentlandite in that it is anisotropic, harder (~ E), and slightly darker bronze yellow. Mineral P occurs as grains in rim troilite peripheries or in troilite blebs in Toluca specimens (Fig. 39). Two grains were analyzed and found to contain Fe, Cr, and S. Compared to troilite, analyses indicated about 35 wt.% Fe and 36-41 wt.% S, which combined with Cr yields a tentative composition of $FeCrS_2$. Mineral P may be a new phase, distinct from compositionally similar daubreelite, $FeCr_2S_4$. It may represent a reaction between Fe(kamacite), FeS(troilite), and $FeCr_2S_4$(daubreelite); (see Ramdohr, 1964).

39. Mineral Q: This phase occurs in the Cosby's Creek specimen as two large (0.3 mm.) rhomboidal grains near the troilite core periphery. It is dark grey, hard (G), and exhibits no internal reflection. Analysis indicates the presence of Cr with very minor Mg. No Fe, Si, or S, or other elements were detected. Mineral Q may be a magnesian chromite. It occurs in pentlanditized troilite, and secondary magnetite and limonite fill the mineral Q-troilite interface. The magnetite appears to replace mineral Q along its edge and magnetite veinlets cut the smaller grain, perhaps as primary magnetite (Fig. 40).

40. Mineral R: This phase is dark grey, hard (G), and possesses prismatic cleavage and a slight brownish internal reflection. Analysis indicates the presence of Ca, Fe, and Si. This phase is probably a Ca-bearing pyroxene. It was observed in the silicate-iron oxide portion of the Trenton cores, occurring in fragmented intergrowths with anorthite and hypersthene.

SUPERIMPOSED SECONDARY TEXTURES

Deformation Textures: Several types of secondary textures were observed in all specimens studied. Two principal types were mechanical deformation and thermal recrystallization. Mechanical deformation includes simple or complex shearing (Fig. 22), brecciation (Figs. 4, 5), complex "squeezed" zones (Fig. 41), and late fracturing (Fig. 19). Thermal alteration is indicated by recrystallization (Fig. 12).

The Hex River specimen is the least deformed, exhibiting only possible thermal recrystallization and late fracturing. The core is a fine grained intergrowth of troilite, manganiferous daubreelite, and mineral F, with segregations of kamacite in the core center (Fig. 2). This core intergrowth may have been homogenized and recrystallized from a previous core, or it may be a unique primary assemblage.

The Magura specimens exhibit the most extensive deformation. Shearing and pressure twinning is common (Fig. 42), but the whole core is essentially a troilite breccia with schreibersite rim fragments included in the core and core troilite "squeezed" into and beyond the schreibersite rim. Throughout the complex breccia, pentlandite alteration of troilite has occurred (Fig. 41).

The Trenton specimens are also relatively deformed. The smaller nodules exhibit pressure twinning and extensive shear zones, which contain alteration pentlandite. The pie-shaped wedges of silicate fragments in an iron oxide matrix occur in the two larger nodules (Fig. 29). The wedges may be primary silicate-sulfide-oxide assemblages, or the angular silicate fragments may have been mechanically included and enclosed in a later iron oxide matrix. Minor shearing and brecciation zones occur in adjacent troilite (Fig. 12), but they are not extensive. The assemblage anorthite-mineral R-troilite-magnetite appears to be compatible with primary meteoritic mineralogy.

The Canyon Diablo specimen exhibits some shearing and pressure twinning zones. The Cosby's Creek specimen exhibits a complex fracture or joint system, along which alteration pentlandite occurs (Fig. 14). The Toluca specimens show extensive but small scale fracturing and shearing. The rim troilite commonly exhibits shear and fracture sets, along which alteration pentlandite and other Fe-Ni-S phases occur (Figs. 11, 22, 37).

Weathering Textures: All specimens show the effects of terrestrial oxidation (weathering). Second magnetite and limonite in most specimens fill major rim boundaries and cut all primary phases (Fig. 19). Some specimens exhibit extensive oxidation zones where the more susceptible phases such as kamacite are replaced by secondary magnetite and limonite (Fig. 10).

TENTATIVE INTERPRETATIONS AND CONCLUSIONS CONCERNING SOME TEXTURAL, STRUCTURAL, AND GENETIC PROBLEMS

Nodule Rim and Core Structure.

The rim-core structure and sequential phase occurrence (Fig. 1) suggest that these nodules were formed in similar environments by similar genetic processes. The nodule rim-core structure may have resulted from elemental diffusion and immiscible liquid segregation as postulated below.

The generally "drop-like" nodule probably segregated as an immiscible Fe-Ni-S-C-P liquid (containing additional minor elements) from the essentially uniform liquid Fe-Ni phase (kamacite). An analogous segregation occurs in the Fe-Ni-S system at high temperatures (Kullerud, 1962). The rim phases crystallized first as suggested by their tendency for external euhedral form (Fig. 3).

The outer rim graphite or cliftonite (perhaps as diamond) crystallized first, as suggested by the perfect euhedral form against adjacent phases (see tentative paragenetic sequence, Fig. 1). Schreibersite, cohenite, and some graphite crystallized as the remaining outer rim, growing into the liquid kamacite as suggested by their external subhedral form. The kamacite generally crystallized subsequent to the C- and P-bearing outer rim, leaving the lower temperature sulfides to form the inner rim and core.

The ferroan sphalerite and rim troilite crystallized before the core phases, as suggested by the inner rim surfaces being "filled" with core phases (Figs. 9, 11, 19). Minerals H and I formed on the core periphery after the inner rim crystallized. The core troilite, with other core phases, probably formed last, as suggested by its large grain size, relative homogeneity, and its "filling" of inner rim irregularities.

Exsolution of Minor Phases Containing Minor Elements.

Minor phases containing minor metallic elements (Co, Cr, Cu, Mn, and some Ni and C) occur either as solid state exsolution laminae along troilite cleavage planes or as grains at the core or rim troilite peripheries (Cr, Mn, Ni, Zn: Fig. 21; Co, Cu: Fig. 13). Similar peripheral occurrences of phases containing minor elements also occur in the silicate- and chlorapatite-enclosed troilite blebs (Fig. 18).

A special case of exsolution is that of the Toluca cores which exhibit extensive graphic intergrowths of troilite and graphite (Figs. 8, 9). The graphite has apparently exsolved along troilite cleavage planes, which implies an original Fe-C-S core phase of up to 50 volume % carbon.

Silicate-Sulfide Intergrowths.

In some Toluca specimens, intergrowths of hypersthene-anorthite-olivine-troilite-graphite-magnetite-chlorapatite occur in "troilite" cores (Fig. 26). Troilite forms abundant exsolution blebs within or along grain boundaries of the silicate phases and myrmekitic intergrowths with hypersthene (Figs. 15, 16). Chlorapatite-magnetite is usually associated with anorthite or occurs as a vein cutting the assemblages. Primary magnetite is also finely intergrown with hypersthene.

The experimental silicate-sulfide reactions studied by Kullerud and Yoder (1963) may offer in part a tentative explanation of these observed assemblages, in that similar assemblages can be produced by a reaction of sulfur (and perhaps high sulfide phases) and high O/Si silicates (e.g., olivine). The contemporaneous formation of the observed assemblages

is suggested by the observed intimate silicate-sulfide-oxide intergrowths noted above. The minor occurrence of olivine suggests such a reaction was incomplete. Kullerud and Yoder point out that minor metallic elements such as Mn, Co, Ni, and Cu form accessory oxides or sulfides. The addition of Cr and Zn would account for the observed minor sulfides. The graphite in these assemblages is probably related to the graphite that is ubiquitous in the Toluca nodules.

The silicate-sulfide-oxide assemblages may represent primary crystallization of these phases, or it may represent the mechanical addition of original silicates to the sulfide nodule.

Two relatively undeformed Trenton troilite cores contain wedges of silicate fragments in an iron oxide matrix. The origin of these wedges is not understood, but their mineralogies are essentially the same as the silicate-sulfide-oxide assemblages discussed above.

Deformation Textures.

Maringer and Manning (1962) describe many types of deformation in iron meteorites, emphasizing shearing, thermal recrystallization, and granulation textures in extra-nodular kamacite and taenite. The nodule deformation textures observed in this study were not compared to such extra-nodular deformation, but such a study should prove informative, as deformation effects are especially evident in sulfide nodules. The observed deformations may be related at least in part to extra-terrestrial phenomena, which Maringer and Manning suggest for most iron meteorites. The postulated thermal diffusion of Ni (see below) and the recrystallization and granulation zones imply a partial reheating. The other deformation textures may also reflect pre-terrestrial events.

Fe-Ni-S Alteration of Troilite and Nickel Metasomatism.

The quantitative compositions, mineralogy, and genesis of pentlandite and other Fe-Ni-S alteration phases is the subject of a subsequent paper in preparation.

Ramdohr (1963), Kullerud (1963), and Mason (1962) consider primary pentlandite a common phase in Ni-rich meteorites. Exsolved primary pentlandite is a minor phase in all specimens studies except Hex River and Canyon Diablo. Kullerud and Ramdohr also refer to a secondary pentlandite formed during weathering.

The distribution of alteration pentlandite was found in this study to be closely related to the nearby presence of primary Ni-bearing phases (e.g., schreibersite). Replacements of kamacite and schreibersite by secondary magnetite and limonite were analyzed in place and showed essentially constant Ni values, suggesting that Ni was fixed in the iron oxides and not subject to weathering transport. In general, the extent of pentlandite alteration bears no relation to the size and extent of oxide veins (Figs. 12,22,40,43,44). The general textures and the fixation of Ni in the iron oxide phases lead to the conclusion that pentlandite and associated Fe-Ni-S alteration phases are not products of terrestrial oxidation and weathering.

The principal alternative to a weathering origin for the Fe-Ni-S alteration phases is through a Ni-diffusion mechanism. These phases (alteration pentlandite; mineral L, "heazlewoodite"; and mineral M) always occur along some zone of deformation or weakness. The abundance of these

phases decreases inward from the rim (Fig. 23), suggesting a Ni source outside the core. In the Toluca rim troilite the Fe-Ni-S phases occur on shear, fracture, or cleavage planes, and are closely associated with adjacent schreibersite (Fig. 37), kamacite, and the nickel minerals H and I (Fig. 33), indicating a Ni source in the direction of these Ni-bearing phases. Excellent examples are shown by extensive Fe-Ni-S alteration adjacent to schreibersite and virtually absent adjacent to Ni-free cohenite (Fig. 24). The extensively altered Magura specimens exhibit an alteration transition of troilite-pentlandite-mineral L ("heazlewoodite")-mineral G ("yellow schreibersite")-schreibersite (Fig. 31), which strongly suggests a metasomatism of Ni across an original core troilite-rim schreibersite interface, during a period of reheating.

In general, the observed textures support the theory of Ni-metasomatism. The most consistent observation is the close association of the troilite Fe-Ni-S alteration phases with nearby Ni-bearing phases. It is tentatively concluded that these alteration phases, pentlandite, mineral L ("heazlewoodite"), and mineral M, were formed by Ni-metasomatism through thermal diffusion of Ni from adjacent Ni-bearing rim phases into Ni-free reactive troilite. The close association between these phases and thermal and mechanical deformation zones suggests that an extra-terrestrial period of thermal reheating and/or mechanical deformation occurred in all but the Hex River and Canyon Diablo specimens.

REFERENCES

Barton, P.B., Toulmin, P. III, (1963), Sphalerite Phase Equilibria in the System Fe-Zn-S: Program, G.S.A. Annual Meeting 1963, pp. 8A-9A.

Bell, P.M., England, J.L., Kullerud, G., (1964), Pressure Effect on Breakdown: Carnegie Inst. Wash. Year Book 63, pp. 206-207.

Boyd, F.R., England, J.L., (1961), Melting of Silicates at High Pressure: Carnegie Inst. Wash. Year Book 60, p. 120.

Brett, P.R., (1963), The Cu-Fe-S System: Carnegie Inst. Wash. Year Book 62, pp. 193-196.

Clark, S.P., Jr., (1961), Iron Meteorites: Carnegie Inst. Wash. Year Book 60, pp. 183-185.

Cohen, E., (1884), Meteoritenkunden; Heft I, Stuttgart, pp. 182-200.

Cohen, E., (1904), Meteoritenkunden; Heft II, Stuttgart, pp. 247-254.

Deer, W.A., Howie, R.A., Zussman, J., (1962), Rock-Forming Minerals, Vol. 1, Ortho- and Ring Silicates: John Wiley & Sons, New York, N.Y., p. 22.

Frondel, C., (1965), Cliftonite in Iron Meteorites: manuscript in preparation.

Frondel, C., Klein, C., (1965), Ureyite, $NaCrSi_2O_6$, a New Meteoritic Pyroxene: Science, in press.

Gehlen, K., (1963), Pyrrhotite Phase Relations at Low Temperatures: Carnegie Inst. Wash. Year Book 62, pp. 213-214.

Keil, K., Fredrikson, K., (1963), Electron Microprobe Analysis of Some Rare Minerals in the Norton County Achondrite: Geochim. et Cosmochim. Acta, v. 27, pp. 939-948.

Kullerud, G., (1960), The Cu_9S_5-Cu_5FeS_4 Join: Carnegie Inst. Wash. Year Book 59, pp. 114-116.

Kullerud, G., (1962), The Fe-Ni-S System: Carnegie Inst. Wash. Year Book 61, pp. 144-150.

Kullerud, G., (1963), The Fe-Ni-S System: Carnegie Inst. Wash. Year Book 62, pp. 175-189.

Kullerud, G., Yoder, H.S., Jr., (1963), Sulfide-Silicate Relations: Carnegie Inst. Wash. Year Book 62, pp. 215-218.

Maringer, R.E., Manning, G.K., (1962), Some Observations on Deformation and Thermal Alterations in Meteoritic Iron; in Researches On Meteorites, ed. C.B. Moore, John Wiley & Sons, New York, pp. 123-144.

Marvin, U.B., Klein, C., Jr., (1964), Meteoritic Zircon: Science, v. 46, pp. 919-920.

Massalski, T.B., (1962), Some Metallurgical Aspects in the Study of Meteorites: in Researches on Meteorites, ed. C.B. Moore, John Wiley & Sons, New York, pp. 107-122.

Mason, B., (1962), Meteorites: John Wiley & Sons, New York, 272 pp.

Perry, S., (1944), The Metallography of Meteoritic Irons: U.S. Natl. Museum Bull. 184, 206 pp.

Ramdohr, P., (1963), The Opaque Minerals in Stony Meteorites: Jour. Geoph. Res., v. 68, pp. 2011-2036.

Ramdohr, P., (1964), Opaque Minerals in Stony Meteorites: Carnegie Inst. Wash. Year Book 63, pp. 217-218.

Short, M.N., (1940), Microscopic Determination of the Ore Minerals: U. S. G. S. Bull. 914, 314 pp.

Winchell, A.N., Winchell, H., (1961), Elements of Optical Mineralogy; Part II, Descriptions of Minerals: 4th Ed.; John Wiley & Sons, New York, pp. 261-302, 405-410, 498-502.

Yund, R.A., Kullerud, G., (1960), The Cu-Fe-S System: Carnegie Inst. Wash. Year Book 59, pp. 111-114.

TABLE I. List of Observed Phases

	Phases	Meteorite Occurrence[1]	Previous Description[2]
	Identified Phases		
1.	Kamacite, ∝-Iron	All	M; P; Rl
2.	Taenite, ɣ-Iron	All	M; P; Rl
3.	Schreibersite	All	M; P; Rl
4.	Cohenite	All	M; P; Rl
5.	Graphite	CC,CD,M,To,Tr	M; P; Rl
5a.	Cliftonite	CC,To	F; M,K
6.	Troilite	All	M; P; Rl
7.	Pyrite	Tr	M
8.	Pentlandite	CC,M,To,Tr	M; Rl
9.	Daubreelite	All	M; P; Rl
10.	Manganiferous daubreelite	CC,CD,HR	K,F
11.	Ferroan sphalerite	To	M?; Rl?
12.	Ferroan alabandite	CD,HR,M,To,Tr	K,F; M; Rl; R2
13.	Native copper	CC,To,Tr	K,F; M; P; Rl
14.	Hypersthene	To,Tr	M,K; M
15.	Olivine	To	M,K; M; P; Rl
16.	Anorthite	To,Tr	M,K; M; P
17.	Ureyite	HR	F,K
18.	Chromite	To	M; P; Rl
19.	Chlorapatite	To	M,K; M
20.	Ilmenite	Tr	M; Rl
21.	Magnetite	All	M; P; Rl
22.	Limonite	All	P; Rl
	Tentatively Identified or Unidentified Phases		
23.	Mineral A (chalcopyrite?)	To	M; Rl
24.	Mineral B (rutile?)	CC,To	M,K
25.	Mineral C (ferroan trevorite?)	To	-
26.	Mineral D (cubanite?)	To	-
27.	Mineral E (bornite?)	To	-
28.	Mineral F	CD,HR,M,To,Tr	-
29.	Mineral G	M,To	-
30.	Mineral H	To	-
31.	Mineral I	To	-
32.	Mineral J	Tr	-
33.	Mineral K	CC,To	-
34.	Mineral L ("heazlewoodite")	CC,M,To,Tr	-
35.	Mineral M	To	-
36.	Mineral N	CD,HR,M,To,Tr	-
37.	Mineral O	To	-
38.	Mineral P	To	-
39.	Mineral Q	CC	-
40.	Mineral R (Ca-pyroxene?)	Tr	M,K; M

[1] CC (Cosby's Creek); CD (Canyon Diablo); HR (Hex River); M (Magura); To (Toluca); Tr (Trenton).

[2] F (Frondel, 1965); F,K (Frondel and Klein, 1965); K,F (Keil and Fredrikson, 1963); M,K (Marvin and Klein, 1964); M (Mason, 1962); P (Perry, 1944); Rl (Ramdohr, 1963); R2 (Ramdohr, 1964).

TABLE II. Observed Compatible and Incompatible Mineral Phase Assemblages and Observed Components

	Cosby's Creek	Canyon Diablo	Hex River	Magura	Toluca	Trenton
I. Compatible Assemblages						
A. Assemblages with troilite:						
1. Cliftonite - cohenite - graphite - kamacite - schreibersite - taenite					X	
2. Cliftonite - cohenite - graphite - kamacite - mineral F - taenite					X	
3. Cohenite - graphite - kamacite - schreibersite - taenite		X			X	
4. Cohenite - graphite - kamacite - mineral F - taenite		X			X	
5. Cohenite - graphite - kamacite - rutile - schreibersite	X					
6. Cohenite - kamacite - schreibersite - taenite		X		X	X	X
7. Cohenite - kamacite - mineral F - taenite		X		X	X	X
8. Cohenite - kamacite - schreibersite			X			
9. Cohenite - kamacite - mineral F			X			
10. Cliftonite - cohenite - ferroan sphalerite - graphite - mineral H - mineral I - schreibersite					X	
11. Anorthite - chlorapatite - chromite - olivine - hypersthene - magnetite - pentlandite - rutile					X	
12. Anorthite - olivine - hypersthene - ilmenite - magnetite - mineral R - pentlandite						X
13. Daubreelite - kamacite - mineral F			X			
14. Daubreelite - magnetite - mineral Q - native copper	X					
15. Daubreelite - ferroan alabandite - native copper - pentlandite						X
16. Daubreelite - ferroan alabandite	X	X	X		X	X
17. Daubreelite	X	X	X	X	X	X
18. Mineral A - mineral D - mineral E - native copper					X	
19. Mineral K	X				X	
20. Manganiferous daubreelite	X	X	X			
21. Ferroan alabandite - mineral O					X	
22. Mineral P					X	
23. Mineral J - pyrite						X
24. Mineral L - mineral M - pentlandite					X	
25. Mineral L - pentlandite	X			X	X	X
26. Pentlandite	X	X		X	X	X
27. Mineral G - mineral L - pentlandite - schreibersite				X		

TABLE II, continued

	Cosby's Creek	Canyon Diablo	Hex River	Magura	Toluca	Trenton
B. Assemblages without troilite:						
1. Limonite - magnetite - mineral C					X	
2. Limonite - magnetite	X	X	X	X	X	X
3. Ferroan sphalerite - mineral N					X	
4. Kamacite - ureyite			X			
II. Incompatible Assemblages						
1. Manganiferous daubreelite / daubreelite	X		X			
2. Ferroan alabandite / manganiferous daubreelite			X		X	
3. Chromite / daubreelite					X	
4. Chromite / mineral P					X	
5. Daubreelite / mineral P					X	
III. Observed Elemental Components						
A. Major components:						
1. Carbon	X	X	X	X	X	X
2. Iron	X	X	X	X	X	X
3. Nickel	X	X	X	X	X	X
4. Oxygen	X	X	X	X	X	X
5. Phosphorus	X	X	X	X	X	X
6. Sulfur	X	X	X	X	X	X
B. Minor components:						
1. Aluminum					X	X
2. Calcium			X		X	X
3. Chlorine					X	
4. Chromium	X	X	X		X	X
5. Cobalt	X				X	
6. Copper	X				X	X
7. Hydrogen	X	X	X	X	X	X
8. Magnesium	X				X	X
9. Manganese	X	X	X		X	
10. Silicon			X		X	X
11. Sodium (?)			X			
12. Titanium	X				X	X
13. Zinc					X	

TABLE III. Combined Diffraction Patterns for Partially Segregated Silicate-Sulfide Intergrowth Mineral Phases

1.			2.		3.		4.		5.		6.		7.		8.		9.	
a.	b.	c.	a.	b.	a.	b.	a.	b.	a.	b.	a.	b.	a.	b.	a.	b.	a.	b.
6.57	1	1	6.52	1														
5.46	1.5	1															5.4	2
5.19	2	3							5.15	2								
4.75	1	2											4.85	4			4.74	1
4.68	1.5	1	4.69	1														
4.62	1	1																
4.51	2	1																
4.42	2	2																
4.03	1	2	4.04	6														
3.93	3	3	3.92	1					3.916	4								
3.80	1	3	3.78	2														
3.75	1.5	1	3.76	1					3.744	1								
3.71	2	1																
			3.62	2.5														
3.53	1.5	3							3.516	3								
			3.47	1					3.481	1								
3.40	9	3	3.37	2.5	3.43	2	3.37	10			3.36	3						
3.33	2.5	1			3.35	3												
3.295	1	2																
3.25	2	3	3.26	5.5											3.245	10		
3.21	6	3	3.21	3.5							3.20	10						
3.19	6	2	3.20	10														
3.17	3	3	3.18	7.5														
3.12	2	2	3.12	4.5	3.09	1												
3.06	1.5	2	3.04	2														
									3.030	1								
3.02	4.5	3					3.00	4	3.014	1								
2.98	3	3									2.98	2					2.98	4
2.96	2.5	1	2.953	2.5									2.966	7				
2.93	2	1	2.935	2														
2.90	5.5	3	2.895	1														
2.89	2	1									2.89	8						

TABLE III, continued

1.			2.		3.		4.		5.		6.		7.		8.		9.	
a.	b.	c.	a.	b.	a.	b.	a.	b.	a.	b.	a.	b.	a.	b.	a.	b.	a.	b.
2.855	1.5	3			2.85	9												
2.814	2	1	2.828	2														
2.792	4	3							2.791	10								
2.754	1.5	1			2.77	10												
2.725	3	3									2.73	3						
2.665	1.5	2	2.655	1	2.65	2											2.66	6
									2.601	10								
2.553	3	2			2.55	1					2.55	5						
2.536	5	3	2.525	2.5					2.533	6			2.530	10			2.52	1
2.485	5	3	2.502	2.5			2.495	4			2.48	5			2.489	4		
2.470	1	1							2.475	6								
2.417	1	2											2.419	1				
2.371	1.5	3							2.370	2								
2.327	2	3																
2.312	1.5	2			2.31	3												
2.292	1.5	2							2.285	3					2.297	1		
2.271	2.5	3							2.270	3								
2.216	1.5	2									2.23	1						
2.176	2	3							2.173	1					2.188	2		
2.127	2	3	2.143	1.5			2.125	4									2.14	1
2.109	2	3									2.11	5						
2.087	2	1											2.096	7			2.09	10
2.039	2	1					2.03	5			2.03	2			2.054	1		
1.973	1.5	2									1.96	4						
1.934	2	1	1.933	1	1.95	5	1.919	3									1.923	3
					1.91	2												
1.886	3	1							1.894	1								
			1.846	1														
1.847	2	1	1.838	2	1.84	5												
1.818	2	2			1.81	2			1.807	1								
1.786	1.5	2									1.78	4						
1.765	1.5	1			1.77	1	1.765	4	1.761	5								
1.758	3	3							1.754	1								

TABLE III, continued

1.			2.		3.		4.		5.		6.		7.		8.		9.	
a.	b.	c.	a.	b.	a.	b.	a.	b.	a.	b.	a.	b.	a.	b.	a.	b.	a.	b.
1.745	1	2							1.743	1							1.748	1
1.714	2.5	1											1.712	6			1.719	5
1.694	1.5	2			1.69	2	1.682	6	1.684	1					1.687	5		
1.644	2	2							1.654	1								
1.627	1	2							1.631	2					1.624	2	1.634	3
1.602	1	3			1.61	1			1.604	1	1.60	6	1.614	8.5				
1.591	2.5	1							1.586	1								
1.528	2	3									1.53	5						
1.502	3	3							1.508	2								
1.492	3	3									1.49	8						
1.481	5	3											1.483	8.5	1.480	1		
																	1.469	3
1.463	1	1																
																	1.445	2
									1.407	1								
1.401	2	3							1.397	1								
											1.39	6						
1.385	2.5	1													1.360	2		
1.351	3.5	1									1.34	3			1.347	1		
1.325	2.5	1											1.327	2			1.331	4
1.311	1	1															1.319	1
1.297	2	1									1.30	5						
1.280	1	2											1.279	3				
1.269	1.5	1									1.27	4	1.264	1				
1.254	1.5	2									1.25	2						
1.235	2	2					1.229	5										

Three diffraction patterns made of mixtures of Toluca silicate-sulfide intergrowth mineral phases. Each mixture pattern represents a partial segregation with respect to hypersthene-anorthite, olivine, or chlorapatite-magnetite. Diffraction patterns made with Cu/K$_\alpha$ radiation with a Ni filter. 1a-9a: observed and reference d-spacings. 1b-9b: measured and reference I/Io. 1c: number of patterns (1-3) on which d-spacings observed. I. Composite of three diffraction patterns. 2. Anorthite, A.S.T.M. #12-301. 3. Chlorapatite, A.S.T.M. #2-851 and J. Drake (Unpub. manuscript, Harvard University, 1965). 4. Graphite, A.S.T.M. #12-212 and Frondel (1965). 5. Olivine, (Mg_2SiO_4 - 64 mol.%), A.S.T.M. #7-159. 6. Hypersthene ($MgSiO_4$ - 70 mol.%), A.S.T.M. #2-520. 7. Magnetite, A.S.T.M. #11-614. 8. Rutile, A.S.T.M. #4-551. 9. Troilite, A.S.T.M. #11-151.

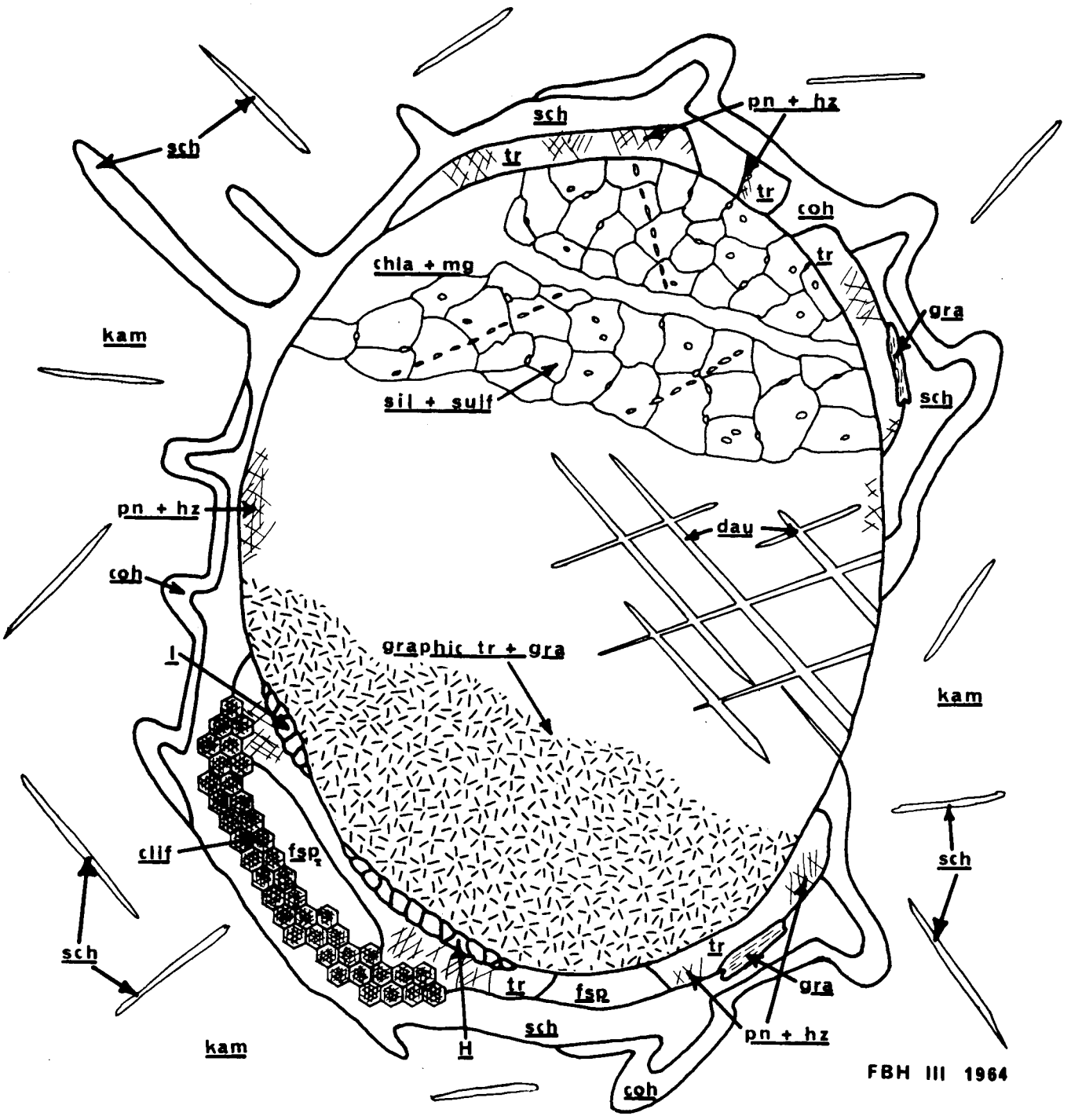

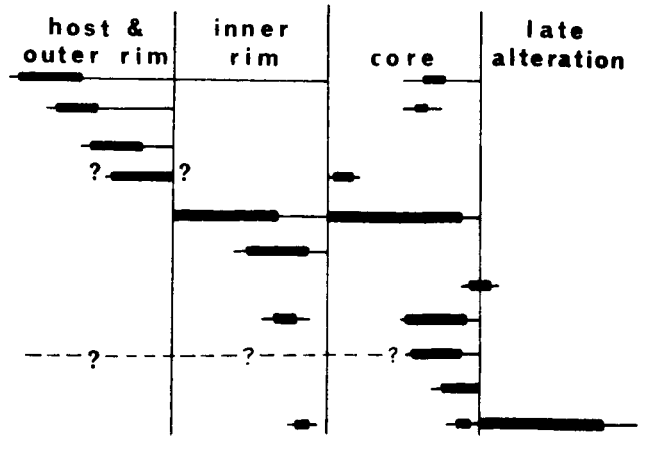

gra(-clif) – graphite (-cliftonite)
sch – schreibersite
coh – cohenite
kam – kamacite
tr – troilite
fsp – ferroan sphalerite
H, l – minerals H, l
dau – daubreélite
sil + sulf – pyroxene, anorthite, troilite
chla + mg – chlorapatite & magnetite
pn + hz – pentlandite & heazlewoodite

FIG. 1. COMPOSITE SKETCH OF NODULE STRUCTURES & TEXTURES, and TENTATIVE TEXTURAL PARAGENETIC SEQUENCE OF PHASES

Figure 2. Hex River (36.5X). Kamacite (kam), manganiferous daubreelite (mdau), mineral F (F), troilite (tr).

Figure 3. Toluca (22.5X). Cohenite (coh), kamacite (kam), schreibersite (sch), troilite (tr).

Figure 4. Toluca (22.5X). Kamacite (kam), magnetite (mg), schreibersite (sch), troilite (tr).

Figure 5. Toluca (200X).

Center of Fig. 4. Magnetite (mg), schreibersite (sch), troilite (tr).

Figure 6. Toluca (36.5X). Anorthite (an), cliftonite (clif), cohenite (coh), graphite (gra), schreibersite (sch), troilite (tr).

Figure 7. Toluca (200X, crossed nichols). Anorthite (an), graphite (gra), hypersthene (hyp).

Figure 8. Toluca (200X, crossed nichols). Daubreelite (dau), ferroan alabandite (fal), graphite (gra), pentlandite (pn), troilite (tr).

Figure 9. Toluca (22.5X). Graphic troilite-graphite intergrowth (grtr), troilite (tr).

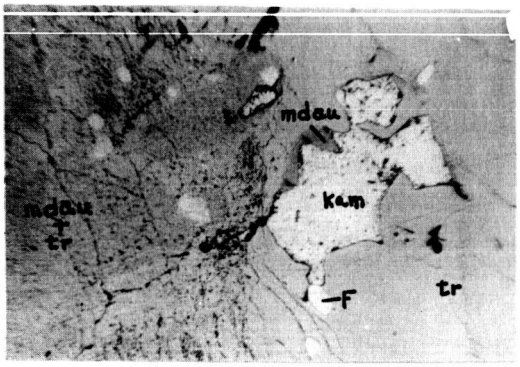

Fig. 2

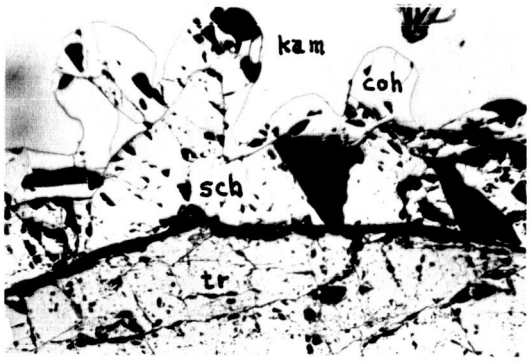

Fig. 3

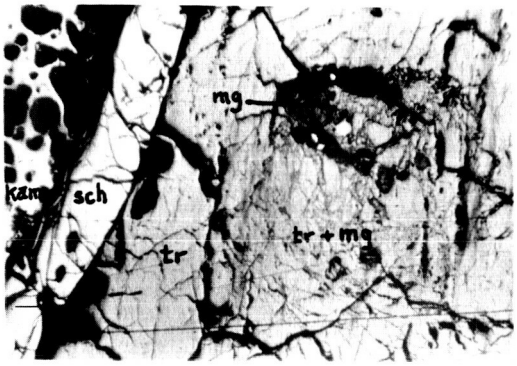

Fig. 4

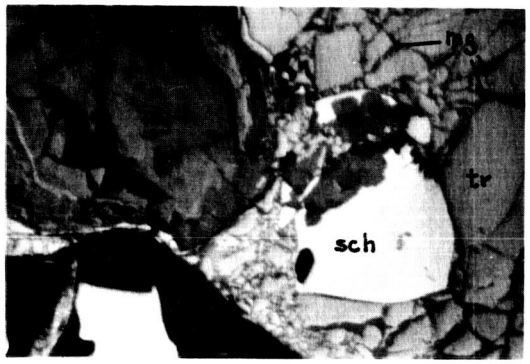

Fig. 5

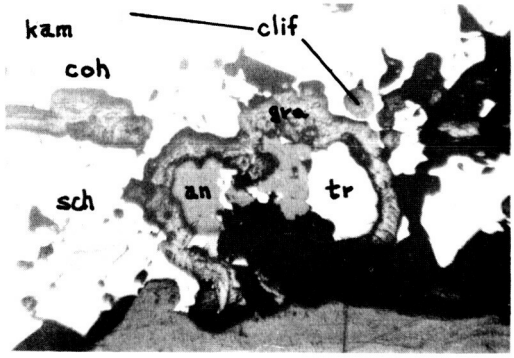

Fig. 6

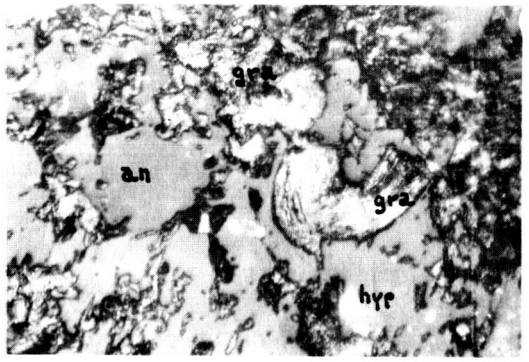

Fig. 7

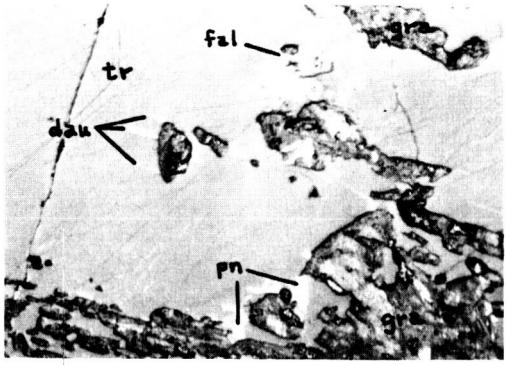

Fig. 8

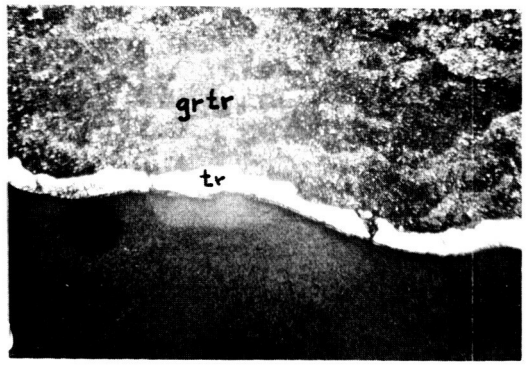

Fig. 9

Figure 10. Toluca (22.5X, crossed nichols). Cliftonite (clif), ferroan sphalerite (fsl), graphic troilite-graphite intergrowth (grtr), kamacite (kam), limonite (lim), magnetite (mg), pentlandite (pn), troilite (tr).

Figure 11. Toluca (100X, crossed nichols). Similar to Fig. 10. Cliftonite (clif), ferroan sphalerite (fsl), graphic troilite-graphite intergrowth (grtr), pentlandite (pn), troilite (tr).

Figure 12. Trenton (100X, crossed nichols). Fragmented silicate-iron oxide intergrowth (left 1/4), magnetite-limonite filled fractures (mg-lim), pentlandite (pn), troilite (tr).

Figure 13. Cosby's Creek (100X). Limonite (lim), mineral K (K), native copper (Cu), pentlandite (pn), troilite (tr).

Figure 14. Cosby's Creek (100X, crossed nichols). Daubreelite (dau), pentlandite (pn), troilite (tr).

Figure 15. Toluca (100X). Anorthite (an), chromite (chr), hypersthene (hyp), mineral B (B), myrmekitic troilite (mtr), schreibersite (sch), troilite (tr).

Figure 16. (700X). Hypersthene (hyp), myrmekitic troilite (mtr).

Figure 17. Toluca (300X). Hypersthene (hyp), troilite (tr).

Fig. 10

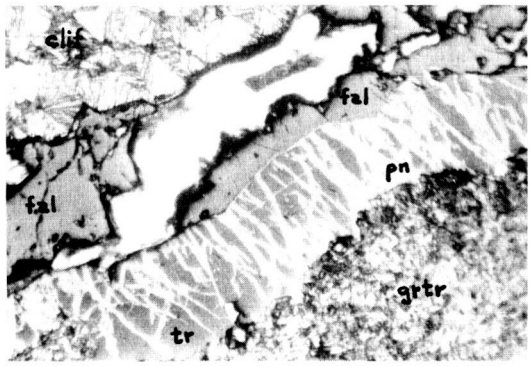

Fig. 11

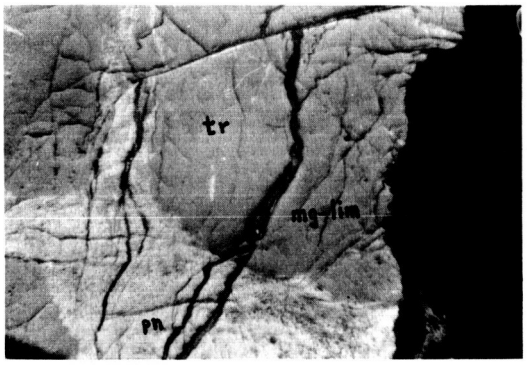

Fig. 12

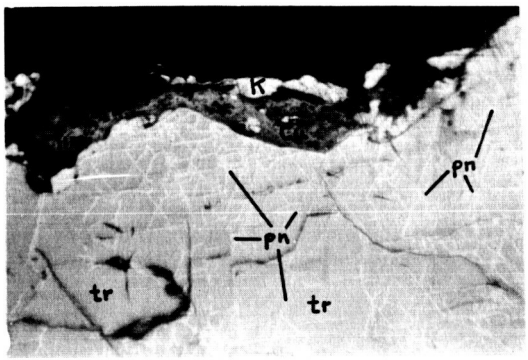

Fig. 13

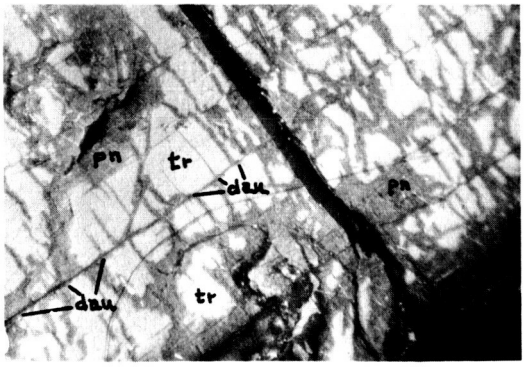

Fig. 14

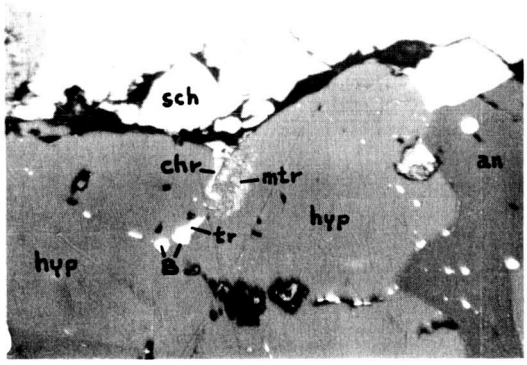

Fig. 15

Fig. 16

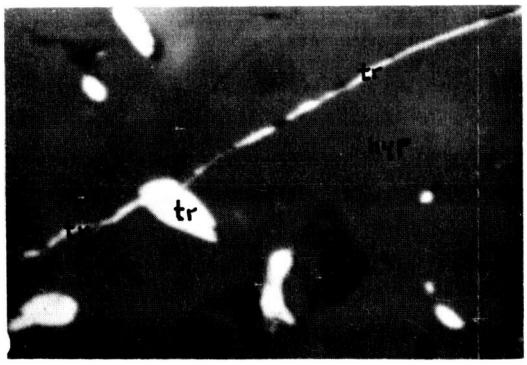

Fig. 17

Figure 18. Toluca (300X). Chlorapatite (chla), daubreelite (dau), ferroan alabandite (fal), graphite (gra), hypersthene (hyp), magnetite (mg), pentlandite (pn), troilite (tr).

Figure 19. Toluca (100X). Graphic troilite-graphite (grtr), magnetite-limonite (mg-lim), minerals H-I (H-I), pentlandite (pn), schreibersite (sch), troilite (tr).

Figure 20. Trenton (100X, crossed nichols). Mineral J (J), pyrite (py), troilite (tr).

Figure 21. Toluca (200X, crossed nichols). Daubreelite (dau), ferroan alabandite (fal), graphite (gra), pentlandite (pn), schreibersite (sch), troilite (tr).

Figure 22. Toluca (100X). Graphic troilite-graphite (grtr), magnetite (mg), pentlandite (pn), troilite (tr).

Figure 23. Magura (200X, crossed nichols). Pentlandite (pn), schreibersite (sch), troilite (tr).

Figure 24. Toluca (100X). Cohenite (coh), pentlandite (pn), schreibersite (sch), troilite (tr).

Figure 25. (700X). Mineral A (A), mineral D (D), mineral E (E), native copper (Cu), troilite (tr).

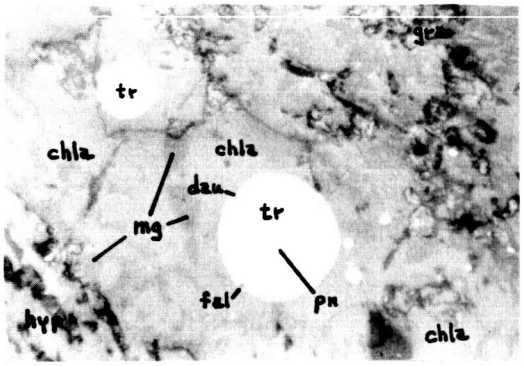

Fig. 18

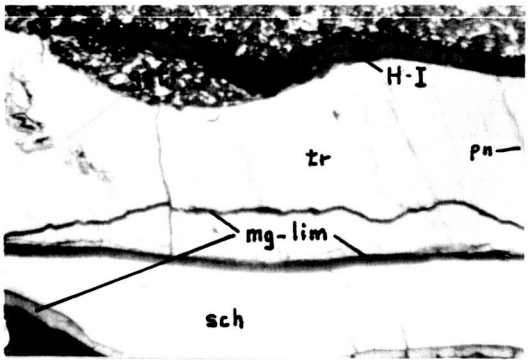

Fig. 19

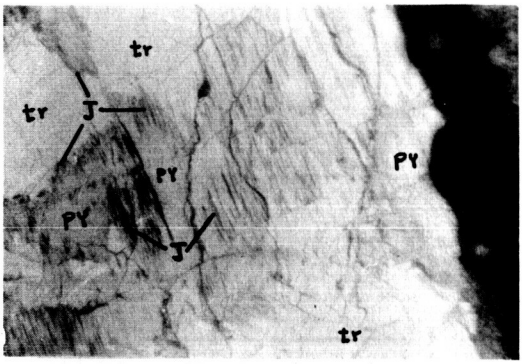

Fig. 20

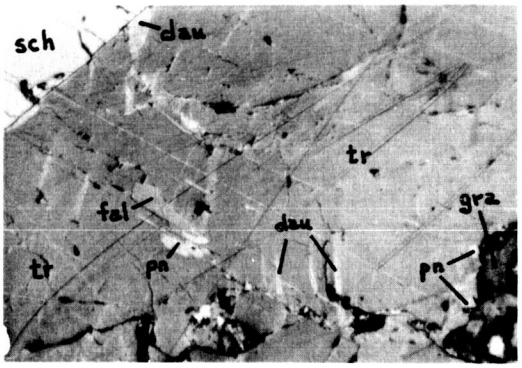

Fig. 21

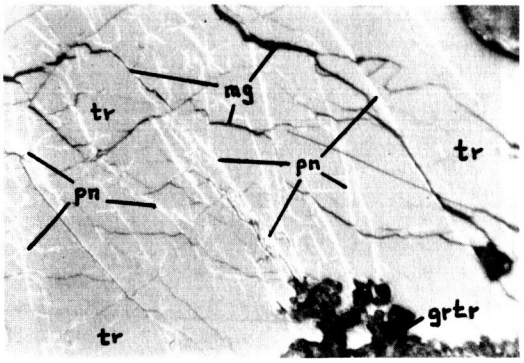

Fig. 22

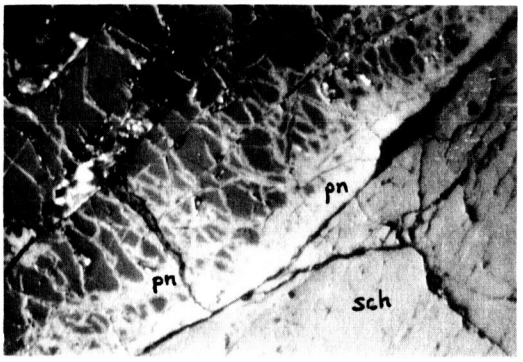

Fig. 23

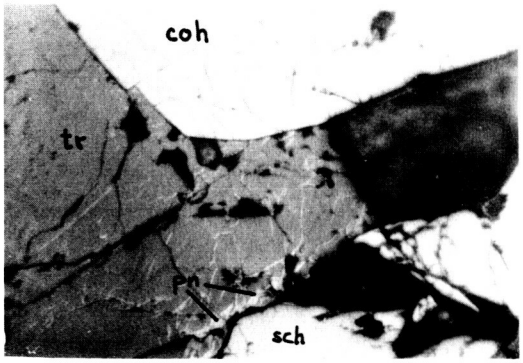

Fig. 24

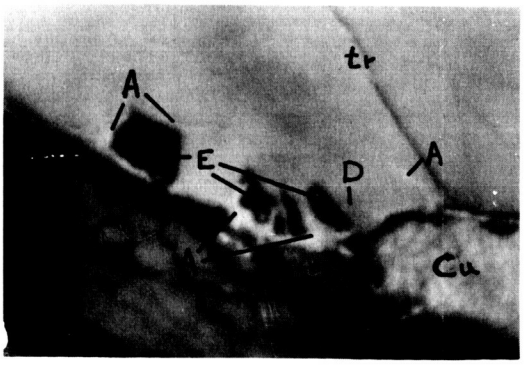

Fig. 25

Figure 26. Toluca (22.5X). Anorthite (an), graphite (gra), hypersthene (hyp), troilite (tr).

Figure 27. Toluca (36.5X). Anorthite (an), chlorapatite (chla), graphite (gra), hypersthene (hyp), magnetite-limonite (mg-lim), troilite (tr).

Figure 28. Toluca (300X). Anorthite (an), hypersthene (hyp), magnetite (mg), mineral B (B), troilite (tr).

Figure 29. Trenton (100X, crossed nichols). Hypersthene (hyp), ilmenite (il), magnetite (mg), silicate fragments-iron oxide intergrowth (sil-ox).

Figure 30. Toluca (100X). Magnetite-limonite (mg-lim), magnetite-mineral C (mg-C).

Figure 31. Magura (200X). Mineral G (G), pentlandite (pn), schreibersite (sch), troilite (tr).

Figure 32. Cosby's Creek (200X). Mineral K (K), pentlandite (pn), troilite (tr).

Figure 33. Toluca (100X). Graphic troilite-graphite (grtr), mineral H (H), mineral L (L), pentlandite (pn), troilite (tr).

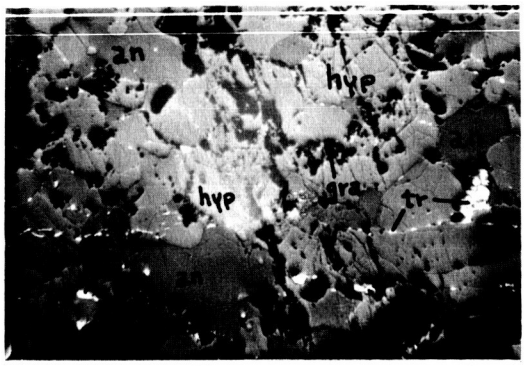

Fig. 26

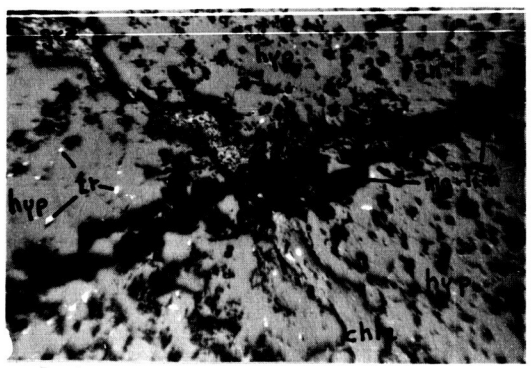

Fig. 27

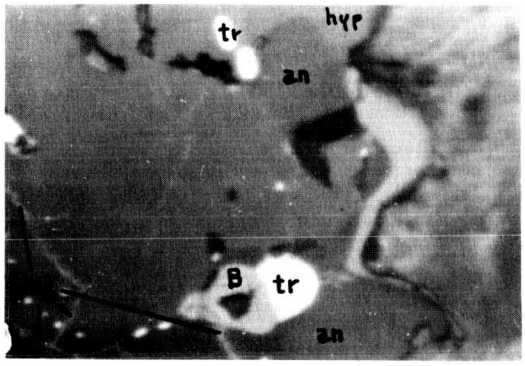

Fig. 28

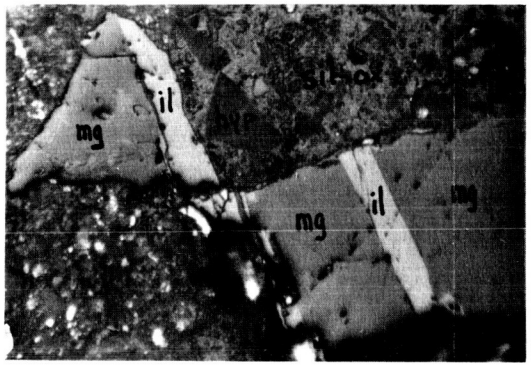

Fig. 29

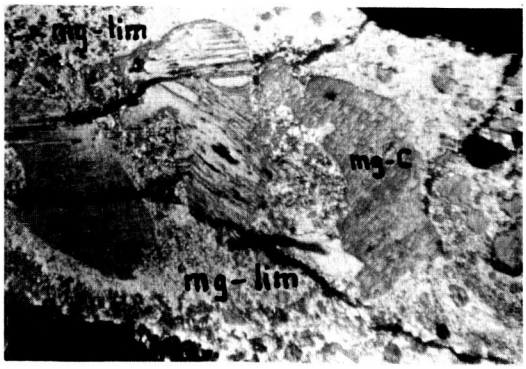

Fig. 30

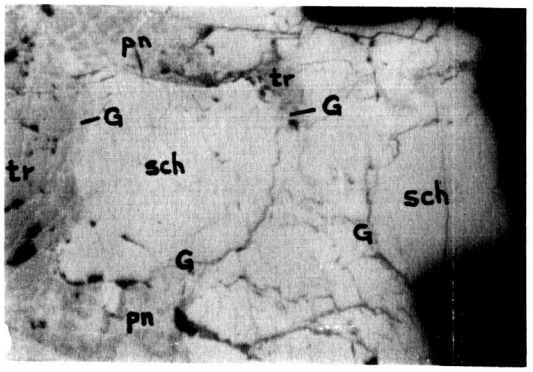

Fig. 31

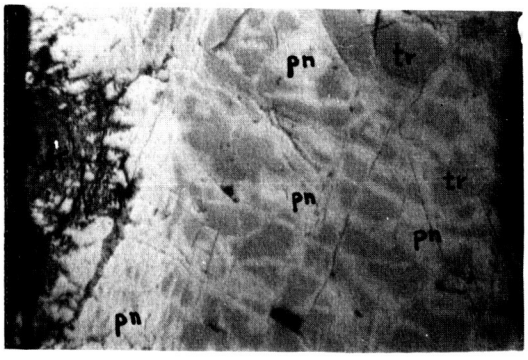

Fig. 32

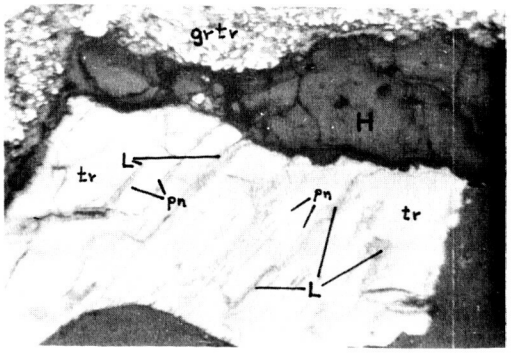

Fig. 33

Figure 34. Toluca (700X).

Center of Figure 33. Magnetite (mg), mineral L (L), pentlandite (pn), troilite (tr).

Figure 35. Toluca (100X). Cohenite (coh), graphic troilite-graphite intergrowth (grtr), mineral H (H), mineral L (L), pentlandite (pn), schreibersite (sch), troilite (tr).

Figure 36. Toluca (100X, crossed nichols). Same as Figure 35, with nichols crossed.

Figure 37. Toluca (200X, crossed nichols). Mineral L (L), mineral M (M), pentlandite (pn), schreibersite (sch), troilite (tr).

Figure 38. Toluca (300X). Cliftonite (clif), ferroan alabandite (fal), graphite (gra), mineral N (N), troilite (tr).

Figure 39. Toluca (300X). Graphite (gra), hypersthene (hyp), mineral P (P), troilite (tr).

Figure 40. Cosby's Creek (100X). Magnetite (mg), mineral R (R), pentlandite (pn), troilite (tr).

Figure 41. Magura (22.5X, crossed nichols). Magnetite-limonite (mg-lim), pentlandite (pn), schreibersite (sch), troilite (tr).

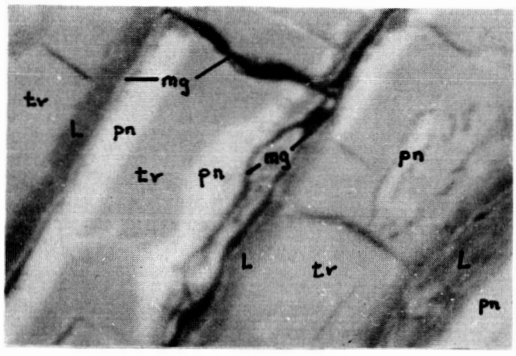

Fig. 34

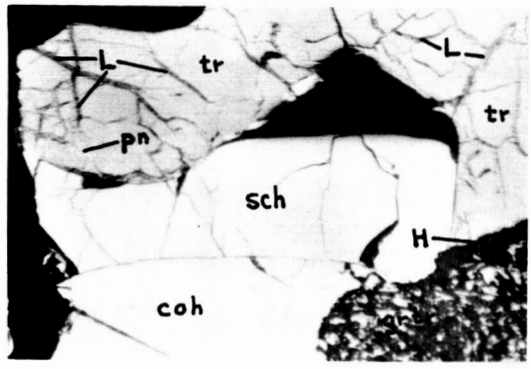

Fig. 35

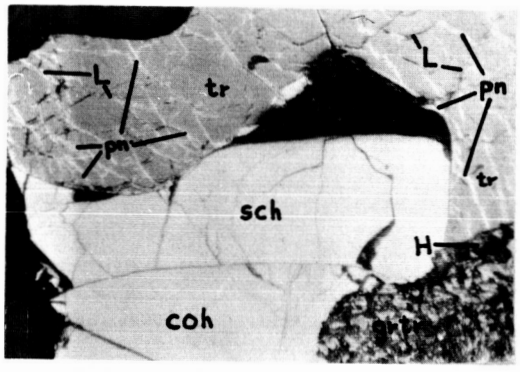

Fig. 36

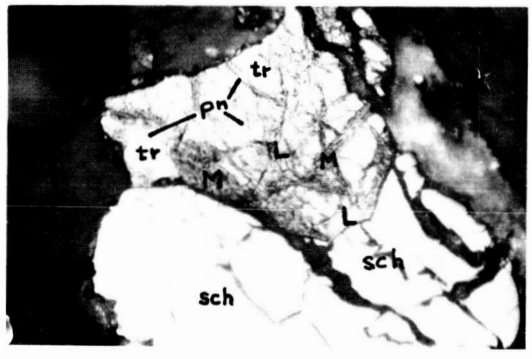

Fig. 37

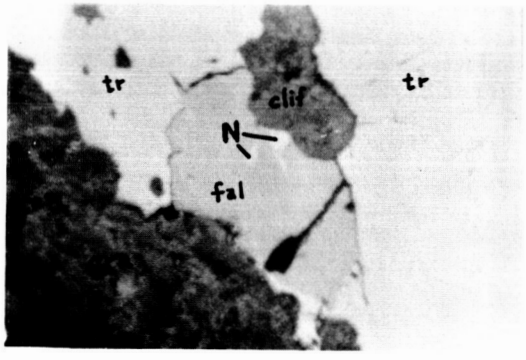

Fig. 38

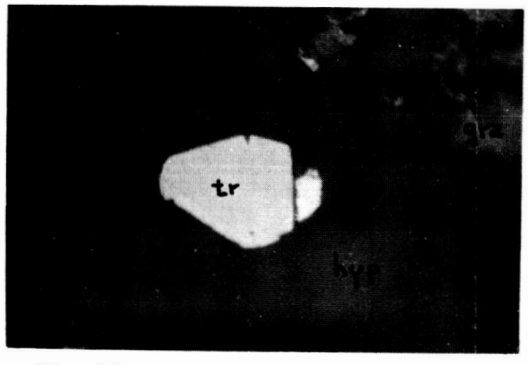

Fig. 39

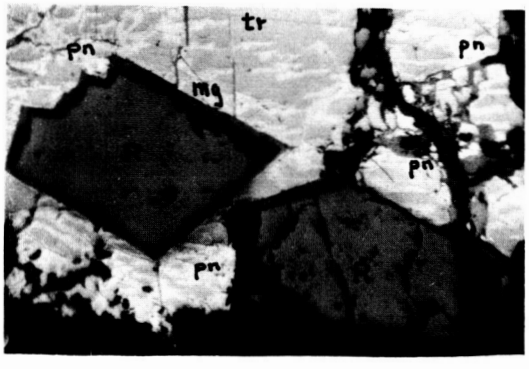

Fig. 40

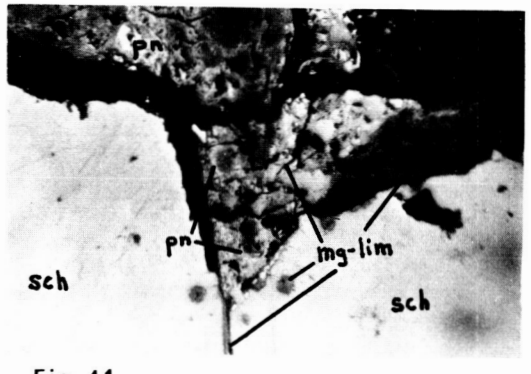

Fig. 41

Figure 42. Magura (100X, crossed nichols). Magnetite-limonite (mg-lim), pentlandite (pn), troilite (tr).

Figure 43. Toluca (36.5X, crossed nichols). Limonite (lim), magnetite (mg), pentlandite (pn), schreibersite (sch), troilite (tr).

Figure 44. Cosby's Creek (200X). Limonite (lim), magnetite (mg), pentlandite (pn), troilite (tr).

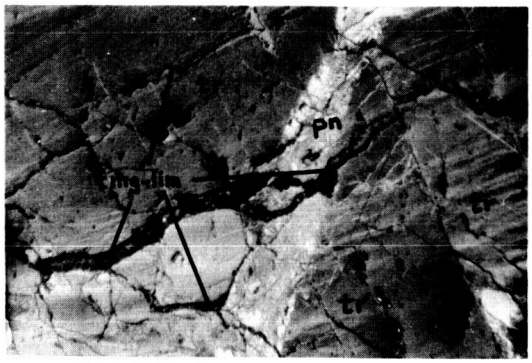

Fig. 42

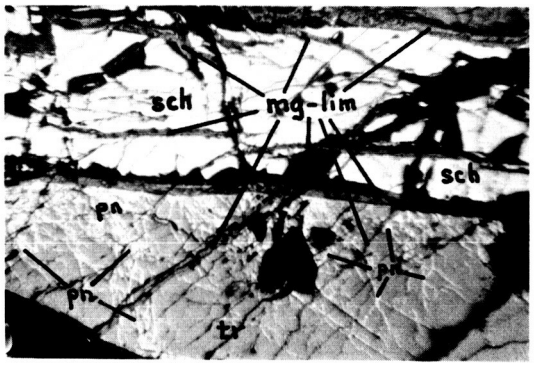

Fig. 43

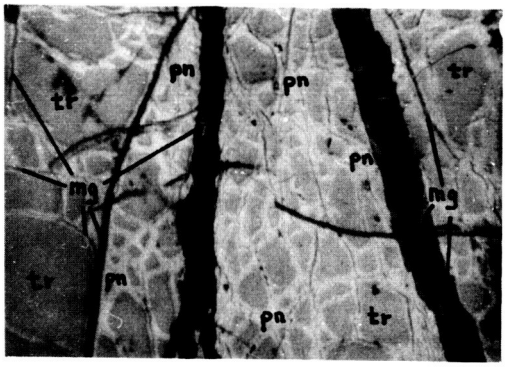

Fig. 44